Aerodynamic Shape Optimization Techniques Based On Control Theory

Antony Jameson[*] and   Juan J. Alonso[†]
Department of Aeronautics & Astronautics
Stanford University
Stanford, California 94305 USA

Abstract

This paper reviews the formulation and application of optimization techniques based on control theory for aerodynamic shape design in both inviscid and viscous compressible flow. The theory is applied to a system defined by the partial differential equations of the flow, with the boundary shape acting as the control. The Frechet derivative of the cost function is determined via the solution of an adjoint partial differential equation, and the boundary shape is then modified in a direction of descent. This process is repeated until an optimum solution is approached. Each design cycle requires the numerical solution of both the flow and the adjoint equations, leading to a computational cost roughly equal to the cost of two flow solutions. Representative results are presented for viscous optimization of transonic wing-body combinations and inviscid optimization of complex configurations.

1   Introduction

The definition of the aerodynamic shapes of modern aircraft relies heavily on computational simulation to enable the rapid evaluation of many alternative designs. Wind tunnel testing is then used to confirm the performance of designs that have been identified by simulation as promising to meet the performance goals. In the case of wing design and propulsion system integration, several complete cycles of computational analysis followed by testing of a preferred design may be used in the evolution of the final configuration. Wind tunnel testing also plays a crucial role in the development of the detailed loads needed to complete the structural design, and in gathering data throughout the flight envelope for the design and verification of the stability and control system. The use of computational simulation to scan many alternative designs has

proved extremely valuable in practice, but it still suffers the limitation that it does not guarantee the identification of the best possible design. Generally one has to accept the best so far by a given cutoff date in the program schedule. To ensure the realization of the true best design, the ultimate goal of computational simulation methods should not just be the analysis of prescribed shapes, but the automatic determination of the true optimum shape for the intended application.

This is the underlying motivation for the combination of computational fluid dynamics with numerical optimization methods. Some of the earliest studies of such an approach were made by Hicks and Henne [1, 2]. The principal obstacle was the large computational cost of determining the sensitivity of the cost function to variations of the design parameters by repeated calculation of the flow. Another way to approach the problem is to formulate aerodynamic shape design within the framework of the mathematical theory for the control of systems governed by partial differential equations [3]. In this view the wing is regarded as a device to produce lift by controlling the flow, and its design is regarded as a problem in the optimal control of the flow equations by changing the shape of the boundary. If the boundary shape is regarded as arbitrary within some requirements of smoothness, then the full generality of shapes cannot be defined with a finite number of parameters, and one must use the concept of the Frechet derivative of the cost with respect to a function. Clearly such a derivative cannot be determined directly by separate variation of each design parameter, because there are now an infinite number of these.

Using techniques of control theory, however, the gradient can be determined indirectly by solving an adjoint equation which has coefficients determined by the solution of the flow equations. This directly corresponds to the gradient technique for trajectory optimization pioneered by Bryson [4]. The cost of solving the adjoint equation is comparable to the cost of solving the flow equations, with the conse-

---

[*] AIAA Fellow, T. V. Jones Professor of Engineering
[†] AIAA Member, Assistant Professor

quence that the gradient with respect to an arbitrarily large number of parameters can be calculated with roughly the same computational cost as two flow solutions. Once the gradient has been calculated, a descent method can be used to determine a shape change which will make an improvement in the design. The gradient can then be recalculated, and the whole process can be repeated until the design converges to an optimum solution, usually within 50 to 100 cycles. The fast calculation of the gradients makes optimization computationally feasible even for designs in three-dimensional viscous flow. There is a possibility that the descent method could converge to a local minimum rather than the global optimum solution. In practice this has not proved a difficulty, provided care is taken in the choice of a cost function which properly reflects the design requirements. Conceptually, with this approach the problem is viewed as infinitely dimensional, with the control being the shape of the bounding surface. Eventually the equations must be discretized for a numerical implementation of the method. For this purpose the flow and adjoint equations may either be separately discretized from their representations as differential equations, or, alternatively, the flow equations may be discretized first, and the discrete adjoint equations then derived directly from the discrete flow equations.

The effectiveness of optimization as a tool for aerodynamic design also depends crucially on the proper choice of cost functions and constraints. One popular approach is to define a target pressure distribution, and then solve the inverse problem of finding the shape that will produce that pressure distribution. Since such a shape does not necessarily exist, direct inverse methods may be ill-posed. This difficulty is removed by reformulating the inverse problem as an optimization problem, in which the deviation between the target and the actual pressure distribution is to be minimized according to a suitable measure such as the surface integral

$$I = \frac{1}{2} \int (p - p_T)^2 d\mathcal{S}$$

where p and p_T are the actual and target pressures. This still leaves the definition of an appropriate pressure architecture to the designer. One may prefer to directly improve suitable performance parameters, for example, to minimize the drag at a given lift and Mach number. In this case it is important to introduce appropriate constraints. For example, if the span is not fixed the vortex drag can be made arbitrarily small by sufficiently increasing the span. In practice, a useful approach is to fix the planform, and optimize the wing sections subject to constraints on minimum thickness.

Studies of the use of control theory for optimum shape design of systems governed by elliptic equations were initiated by Pironneau [5]. The control theory approach to optimal aerodynamic design was first applied to transonic flow by Jameson [6, 7, 8, 9, 10, 11]. He formulated the method for inviscid compressible flows with shock waves governed by both the potential flow and the Euler equations [7]. Numerical results showing the method to be extremely effective for the design of airfoils in transonic potential flow were presented in [12], and for three-dimensional wing design using the Euler equations in [13]. More recently the method has been employed for the shape design of complex aircraft configurations [14, 15], using a grid perturbation approach to accommodate the geometry modifications. The method has been used to support the aerodynamic design studies of several industrial projects, including the Beech Premier and the McDonnell Douglas MDXX and Blended Wing-Body projects. The application to the MDXX is described in [9]. The experience gained in these industrial applications made it clear that the viscous effects cannot be ignored in transonic wing design, and the method has therefore been extended to treat the Reynolds Averaged Navier-Stokes equations [11]. Adjoint methods have also been the subject of studies by a number of other authors, including Baysal and Eleshaky [16], Huan and Modi [17], Desai and Ito [18], Anderson and Venkatakrishnan [19], and Peraire and Elliot [20].

This paper reviews the formulation and development of the compressible viscous adjoint equations, and presents some examples of recent applications of design techniques based on control theory to viscous transonic wing design, and also to transonic and supersonic wing design for complex configurations.

2 General Formulation of the Adjoint Approach to Optimal Design

Before embarking on a detailed derivation of the adjoint formulation for optimal design using the Navier–Stokes equations, it is helpful to summarize the general abstract description of the adjoint approach which has been thoroughly documented in references [7, 21].

The progress of the design procedure is measured in terms of a cost function I, which could be, for example the drag coefficient or the lift to drag ratio. For flow about an airfoil or wing, the aerodynamic

properties which define the cost function are functions of the flow-field variables (w) and the physical location of the boundary, which may be represented by the function $\mathcal{F}$, say. Then

$$I = I\left(w, \mathcal{F}\right),$$

and a change in $\mathcal{F}$ results in a change

$$\delta I = \left[\frac{\partial I^T}{\partial w}\right]_I \delta w + \left[\frac{\partial I^T}{\partial \mathcal{F}}\right]_{II} \delta \mathcal{F}, \qquad (1)$$

in the cost function. Here, the subscripts I and II are used to distinguish the contributions due to the variation δw in the flow solution from the change associated directly with the modification $\delta \mathcal{F}$ in the shape. This notation is introduced to assist in grouping the numerous terms that arise during the derivation of the full Navier–Stokes adjoint operator, so that it remains feasible to recognize the basic structure of the approach as it is sketched in the present section.

Using control theory, the governing equations of the flow field are introduced as a constraint in such a way that the final expression for the gradient does not require multiple flow solutions. This corresponds to eliminating δw from (1).

Suppose that the governing equation R which expresses the dependence of w and $\mathcal{F}$ within the flow-field domain $\mathcal{D}$ can be written as

$$R\left(w, \mathcal{F}\right) = 0. \qquad (2)$$

Then δw is determined from the equation

$$\delta R = \left[\frac{\partial R}{\partial w}\right]_I \delta w + \left[\frac{\partial R}{\partial \mathcal{F}}\right]_{II} \delta \mathcal{F} = 0. \qquad (3)$$

Next, introducing a Lagrange Multiplier ψ, we have

$$\delta I = \frac{\partial I^T}{\partial w}\delta w + \frac{\partial I^T}{\partial \mathcal{F}}\delta \mathcal{F} - \psi^T \left(\left[\frac{\partial R}{\partial w}\right]\delta w + \left[\frac{\partial R}{\partial \mathcal{F}}\right]\delta \mathcal{F}\right)$$
$$= \left\{\frac{\partial I^T}{\partial w} - \psi^T\left[\frac{\partial R}{\partial w}\right]\right\}_I \delta w + \left\{\frac{\partial I^T}{\partial \mathcal{F}} - \psi^T\left[\frac{\partial R}{\partial \mathcal{F}}\right]\right\}_{II} \delta \mathcal{F}. \quad (4)$$

Choosing ψ to satisfy the adjoint equation

$$\left[\frac{\partial R}{\partial w}\right]^T \psi = \frac{\partial I}{\partial w} \qquad (5)$$

the first term is eliminated, and we find that

$$\delta I = \mathcal{G}\delta \mathcal{F}, \qquad (6)$$

where

$$\mathcal{G} = \frac{\partial I^T}{\partial \mathcal{F}} - \psi^T \left[\frac{\partial R}{\partial \mathcal{F}}\right].$$

The advantage is that (6) is independent of δw, with the result that the gradient of I with respect

to an arbitrary number of design variables can be determined without the need for additional flow-field evaluations. In the case that (2) is a partial differential equation, the adjoint equation (5) is also a partial differential equation and determination of the appropriate boundary conditions requires careful mathematical treatment.

The computational cost of a single design cycle is roughly equivalent to the cost of two flow solutions since the the adjoint problem has similar complexity. When the number of design variables becomes large, the computational efficiency of the control theory approach over traditional approach, which requires direct evaluation of the gradients by individually varying each design variable and recomputing the flow field, becomes compelling.

Once equation (3) is established, an improvement can be made with a shape change

$$\delta \mathcal{F} = -\lambda \mathcal{G}$$

where λ is positive, and small enough that the first variation is an accurate estimate of δI. The variation in the cost function then becomes

$$\delta I = -\lambda \mathcal{G}^T \mathcal{G} < 0.$$

After making such a modification, the flow field and corresponding gradient can be recalculated and the process repeated to follow a path of steepest descent until a minimum is reached. In order to avoid violating constraints, such as a minimum acceptable wing thickness, the gradient may be projected into an allowable subspace within which the constraints are satisfied. In this way, procedures can be devised which must necessarily converge at least to a local minimum.

3 The Navier-Stokes Equations

For the derivations that follow, it is convenient to use Cartesian coordinates (x_1, x_2, x_3) and to adopt the convention of indicial notation where a repeated index "i" implies summation over $i = 1$ to 3. The three-dimensional Navier-Stokes equations then take the form

$$\frac{\partial w}{\partial t} + \frac{\partial f_i}{\partial x_i} = \frac{\partial f_{vi}}{\partial x_i} \quad \text{in } \mathcal{D}, \qquad (7)$$

where the state vector w, inviscid flux vector f and viscous flux vector f_v are described respectively by

$$w = \left\{\begin{array}{c} \rho \\ \rho u_1 \\ \rho u_2 \\ \rho u_3 \\ \rho E \end{array}\right\}, \qquad (8)$$

$$f_i = \left\{ \begin{array}{c} \rho u_i \\ \rho u_i u_1 + p\delta_{i1} \\ \rho u_i u_2 + p\delta_{i2} \\ \rho u_i u_3 + p\delta_{i3} \\ \rho u_i H \end{array} \right\}, \qquad (9)$$

$$f_{vi} = \left\{ \begin{array}{c} 0 \\ \sigma_{ij}\delta_{j1} \\ \sigma_{ij}\delta_{j2} \\ \sigma_{ij}\delta_{j3} \\ u_j\sigma_{ij} + k\frac{\partial T}{\partial x_i} \end{array} \right\}. \qquad (10)$$

In these definitions, ρ is the density, u_1, u_2, u_3 are the Cartesian velocity components, E is the total energy and δ_{ij} is the Kronecker delta function. The pressure is determined by the equation of state

$$p = (\gamma - 1)\rho \left\{ E - \frac{1}{2}(u_i u_i) \right\},$$

and the stagnation enthalpy is given by

$$H = E + \frac{p}{\rho},$$

where γ is the ratio of the specific heats. The viscous stresses may be written as

$$\sigma_{ij} = \mu \left(\frac{\partial u_i}{\partial x_j} + \frac{\partial u_j}{\partial x_i} \right) + \lambda\delta_{ij}\frac{\partial u_k}{\partial x_k}, \qquad (11)$$

where μ and λ are the first and second coefficients of viscosity. The coefficient of thermal conductivity and the temperature are computed as

$$k = \frac{c_p \mu}{Pr}, \qquad T = \frac{p}{R\rho}, \qquad (12)$$

where Pr is the Prandtl number, c_p is the specific heat at constant pressure, and R is the gas constant.

For discussion of real applications using a discretization on a body conforming structured mesh, it is also useful to consider a transformation to the computational coordinates (ξ_1, ξ_2, ξ_3) defined by the metrics

$$K_{ij} = \left[\frac{\partial x_i}{\partial \xi_j} \right], \quad J = \det(K), \quad K_{ij}^{-1} = \left[\frac{\partial \xi_i}{\partial x_j} \right].$$

The Navier-Stokes equations can then be written in computational space as

$$\frac{\partial(Jw)}{\partial t} + \frac{\partial(F_i - F_{vi})}{\partial \xi_i} = 0 \quad \text{in } \mathcal{D}, \qquad (13)$$

where the inviscid and viscous flux contributions are now defined with respect to the computational cell faces by $F_i = S_{ij}f_j$ and $F_{vi} = S_{ij}f_{vj}$, and

the quantity $S_{ij} = JK_{ij}^{-1}$ represents the projection of the ξ_i cell face along the x_j axis. In obtaining equation (13) we have made use of the property that

$$\frac{\partial S_{ij}}{\partial \xi_i} = 0 \qquad (14)$$

which represents the fact that the sum of the face areas over a closed volume is zero, as can be readily verified by a direct examination of the metric terms.

4 Formulation of the Optimal Design Problem for the Navier-Stokes Equations

Aerodynamic optimization is based on the determination of the effect of shape modifications on some performance measure which depends on the flow. For convenience, the coordinates ξ_i describing the fixed computational domain are chosen so that each boundary conforms to a constant value of one of these coordinates. Variations in the shape then result in corresponding variations in the mapping derivatives defined by K_{ij}.

Suppose that the performance is measured by a cost function

$$I = \int_{\mathcal{B}} \mathcal{M}(w, S) \, d\mathcal{B}_\xi + \int_{\mathcal{D}} \mathcal{P}(w, S) \, d\mathcal{D}_\xi,$$

containing both boundary and field contributions where $d\mathcal{B}_\xi$ and $d\mathcal{D}_\xi$ are the surface and volume elements in the computational domain. In general, $\mathcal{M}$ and $\mathcal{P}$ will depend on both the flow variables w and the metrics S defining the computational space. In the case of a multi-point design the flow variables may be separately calculated for several different conditions of interest.

The design problem is now treated as a control problem where the boundary shape represents the control function, which is chosen to minimize I subject to the constraints defined by the flow equations (13). A shape change produces a variation in the flow solution δw and the metrics δS which in turn produce a variation in the cost function

$$\delta I = \int_{\mathcal{B}} \delta\mathcal{M}(w, S) \, d\mathcal{B}_\xi + \int_{\mathcal{D}} \delta\mathcal{P}(w, S) \, d\mathcal{D}_\xi, \quad (15)$$

with

$$\begin{array}{rcl} \delta\mathcal{M} &=& [\mathcal{M}_w]_I \, \delta w + \delta\mathcal{M}_{II}, \\ \delta\mathcal{P} &=& [\mathcal{P}_w]_I \, \delta w + \delta\mathcal{P}_{II}, \end{array} \qquad (16)$$

where we continue to use the subscripts I and II to distinguish between the contributions associated

with the variation of the flow solution δw and those associated with the metric variations δS. Thus $[\mathcal{M}_w]_I$ and $[\mathcal{P}_w]_I$ represent $\frac{\partial \mathcal{M}}{\partial w}$ and $\frac{\partial \mathcal{P}}{\partial w}$ with the metrics fixed, while $\delta \mathcal{M}_{II}$ and $\delta \mathcal{P}_{II}$ represent the contribution of the metric variations δS to $\delta \mathcal{M}$ and $\delta \mathcal{P}$.

In the steady state, the constraint equation (13) specifies the variation of the state vector δw by

$$\frac{\partial}{\partial \xi_i} \delta \left(F_i - F_{vi} \right) = 0. \qquad (17)$$

Here δF_i and δF_{vi} can also be split into contributions associated with δw and δS using the notation

$$\begin{aligned} \delta F_i &= \left[F_{iw} \right]_I \delta w + \delta F_{iII} \\ \delta F_{vi} &= \left[F_{viw} \right]_I \delta w + \delta F_{viII}. \end{aligned} \qquad (18)$$

The inviscid contributions are easily evaluated as

$$\left[F_{iw} \right]_I = S_{ij} \frac{\partial f_j}{\partial w}, \quad \delta F_{iII} = \delta S_{ij} f_j.$$

The details of the viscous contributions are complicated by the additional level of derivatives in the stress and heat flux terms and will be derived in Section 6. Multiplying by a co-state vector ψ, which will play an analogous role to the Lagrange multiplier introduced in equation (4), and integrating over the domain produces

$$\int_{\mathcal{D}} \psi^T \frac{\partial}{\partial \xi_i} \delta \left(F_i - F_{vi} \right) = 0. \qquad (19)$$

If ψ is differentiable this may be integrated by parts to give

$$\int_{\mathcal{B}} n_i \psi^T \delta \left(F_i - F_{vi} \right) d\mathcal{B}_\xi$$
$$- \int_{\mathcal{D}} \frac{\partial \psi^T}{\partial \xi_i} \delta \left(F_i - F_{vi} \right) d\mathcal{D}_\xi = 0. \qquad (20)$$

Since the left hand expression equals zero, it may be subtracted from the variation in the cost function (15) to give

$$\begin{aligned} \delta I &= \int_{\mathcal{B}} \left[\delta \mathcal{M} - n_i \psi^T \delta \left(F_i - F_{vi} \right) \right] d\mathcal{B}_\xi \\ &+ \int_{\mathcal{D}} \left[\delta \mathcal{P} + \frac{\partial \psi^T}{\partial \xi_i} \delta \left(F_i - F_{vi} \right) \right] d\mathcal{D}_\xi. \end{aligned} \qquad (21)$$

Now, since ψ is an arbitrary differentiable function, it may be chosen in such a way that δI no longer depends explicitly on the variation of the state vector δw. The gradient of the cost function can then be evaluated directly from the metric variations without having to recompute the variation δw resulting from the perturbation of each design variable.

Comparing equations (16) and (18), the variation δw may be eliminated from (21) by equating all field terms with subscript "I" to produce a differential adjoint system governing ψ

$$\frac{\partial \psi^T}{\partial \xi_i} \left[F_{iw} - F_{viw} \right]_I + \mathcal{P}_w = 0 \quad \text{in } \mathcal{D}. \qquad (22)$$

The corresponding adjoint boundary condition is produced by equating the subscript "I" boundary terms in equation (21) to produce

$$n_i \psi^T \left[F_{iw} - F_{viw} \right]_I = \mathcal{M}_w \quad \text{on } \mathcal{B}. \qquad (23)$$

The remaining terms from equation (21) then yield a simplified expression for the variation of the cost function which defines the gradient

$$\begin{aligned} \delta I &= \int_{\mathcal{B}} \left\{ \delta \mathcal{M}_{II} - n_i \psi^T \left[\delta F_i - \delta F_{vi} \right]_{II} \right\} d\mathcal{B}_\xi \\ &+ \int_{\mathcal{D}} \left\{ \delta \mathcal{P}_{II} + \frac{\partial \psi^T}{\partial \xi_i} \left[\delta F_i - \delta F_{vi} \right]_{II} \right\} d\mathcal{D}_\xi. \end{aligned} \qquad (24)$$

The details of the formula for the gradient depend on the way in which the boundary shape is parameterized as a function of the design variables, and the way in which the mesh is deformed as the boundary is modified. Using the relationship between the mesh deformation and the surface modification, the field integral is reduced to a surface integral by integrating along the coordinate lines emanating from the surface. Thus the expression for δI is finally reduced to the form of equation (6)

$$\delta I = \int_{\mathcal{B}} \mathcal{G} \delta \mathcal{F} \, d\mathcal{B}_\xi$$

where $\mathcal{F}$ represents the design variables, and $\mathcal{G}$ is the gradient, which is a function defined over the boundary surface.

The boundary conditions satisfied by the flow equations restrict the form of the left hand side of the adjoint boundary condition (23). Consequently, the boundary contribution to the cost function $\mathcal{M}$ cannot be specified arbitrarily. Instead, it must be chosen from the class of functions which allow cancellation of all terms containing δw in the boundary integral of equation (21). On the other hand, there is no such restriction on the specification of the field contribution to the cost function $\mathcal{P}$, since these terms may always be absorbed into the adjoint field equation (22) as source terms.

It is convenient to develop the inviscid and viscous contributions to the adjoint equations separately. Also, for simplicity, it will be assumed that the portion of the boundary that undergoes shape modifications is restricted to the coordinate surface

$\xi_2 = 0$. Then equations (21) and (23) may be simplified by incorporating the conditions

$$n_1 = n_3 = 0, \quad n_2 = 1, \quad d\mathcal{B}_\xi = d\xi_1 d\xi_3,$$

so that only the variations δF_2 and δF_{v2} need to be considered at the wall boundary.

5 Derivation of the Inviscid Adjoint Terms

The inviscid contributions have been previously derived in [12, 22] but are included here for completeness. Taking the transpose of equation (22), the inviscid adjoint equation may be written as

$$C_i^T \frac{\partial \psi}{\partial \xi_i} = 0 \quad \text{in } \mathcal{D}, \tag{25}$$

where the inviscid Jacobian matrices in the transformed space are given by

$$C_i = S_{ij} \frac{\partial f_j}{\partial w}.$$

The transformed velocity components have the form

$$U_i = S_{ij} u_j,$$

and the condition that there is no flow through the wall boundary at $\xi_2 = 0$ is equivalent to

$$U_2 = 0,$$

so that

$$\delta U_2 = 0$$

when the boundary shape is modified. Consequently the variation of the inviscid flux at the boundary reduces to

$$\delta F_2 = \delta p \left\{ \begin{array}{c} 0 \\ S_{21} \\ S_{22} \\ S_{23} \\ 0 \end{array} \right\} + p \left\{ \begin{array}{c} 0 \\ \delta S_{21} \\ \delta S_{22} \\ \delta S_{23} \\ 0 \end{array} \right\}. \tag{26}$$

Since δF_2 depends only on the pressure, it is now clear that the performance measure on the boundary $\mathcal{M}(w, S)$ may only be a function of the pressure and metric terms. Otherwise, complete cancellation of the terms containing δw in the boundary integral would be impossible. One may, for example, include arbitrary measures of the forces and moments in the cost function, since these are functions of the surface pressure.

In order to design a shape which will lead to a desired pressure distribution, a natural choice is to set

$$I = \frac{1}{2} \int_\mathcal{B} (p - p_d)^2 \, dS$$

where p_d is the desired surface pressure, and the integral is evaluated over the actual surface area. In the computational domain this is transformed to

$$I = \frac{1}{2} \iint_{\mathcal{B}_w} (p - p_d)^2 \, |S_2| \, d\xi_1 d\xi_3,$$

where the quantity

$$|S_2| = \sqrt{S_{2j} S_{2j}}$$

denotes the face area corresponding to a unit element of face area in the computational domain. Now, to cancel the dependence of the boundary integral on δp, the adjoint boundary condition reduces to

$$\psi_j n_j = p - p_d \tag{27}$$

where n_j are the components of the surface normal

$$n_j = \frac{S_{2j}}{|S_2|}.$$

This amounts to a transpiration boundary condition on the co-state variables corresponding to the momentum components. Note that it imposes no restriction on the tangential component of ψ at the boundary.

In the presence of shock waves, neither p nor p_d are necessarily continuous at the surface. The boundary condition is then in conflict with the assumption that ψ is differentiable. This difficulty can be circumvented by the use of a smoothed boundary condition [22].

6 Derivation of the Viscous Adjoint Terms

In computational coordinates, the viscous terms in the Navier–Stokes equations have the form

$$\frac{\partial F_{vi}}{\partial \xi_i} = \frac{\partial}{\partial \xi_i} \left(S_{ij} f_{vj} \right).$$

Computing the variation δw resulting from a shape modification of the boundary, introducing a co-state vector ψ and integrating by parts following the steps outlined by equations (17) to (20) produces

$$\int_\mathcal{B} \psi^T \left(\delta S_{2j} f_{vj} + S_{2j} \delta f_{vj} \right) d\mathcal{B}_\xi$$

$$- \int_\mathcal{D} \frac{\partial \psi^T}{\partial \xi_i} \left(\delta S_{ij} f_{vj} + S_{ij} \delta f_{vj} \right) d\mathcal{D}_\xi,$$

where the shape modification is restricted to the coordinate surface $\xi_2 = 0$ so that $n_1 = n_3 = 0$, and $n_2 = 1$. Furthermore, it is assumed that the boundary contributions at the far field may either be neglected or else eliminated by a proper choice of boundary conditions as previously shown for the inviscid case [12, 22].

The viscous terms will be derived under the assumption that the viscosity and heat conduction coefficients μ and k are essentially independent of the flow, and that their variations may be neglected. This simplification has been successfully used for may aerodynamic problems of interest. In the case of some turbulent flows, there is the possibility that the flow variations could result in significant changes in the turbulent viscosity, and it may then be necessary to account for its variation in the calculation.

Transformation to Primitive Variables

The derivation of the viscous adjoint terms is simplified by transforming to the primitive variables

$$\tilde{w}^T = (\rho, u_1, u_2, u_3, p)^T,$$

because the viscous stresses depend on the velocity derivatives $\frac{\partial u_i}{\partial x_j}$, while the heat flux can be expressed as

$$\kappa \frac{\partial}{\partial x_i} \left(\frac{p}{\rho} \right).$$

where $\kappa = \frac{k}{R} = \frac{\gamma \mu}{Pr(\gamma - 1)}$. The relationship between the conservative and primitive variations is defined by the expressions

$$\delta w = M \delta \tilde{w}, \quad \delta \tilde{w} = M^{-1} \delta w$$

which make use of the transformation matrices $M = \frac{\partial w}{\partial \tilde{w}}$ and $M^{-1} = \frac{\partial \tilde{w}}{\partial w}$. These matrices are provided in transposed form for future convenience

$$M^T = \begin{bmatrix} 1 & u_1 & u_2 & u_3 & \frac{u_i u_i}{2} \\ 0 & \rho & 0 & 0 & \rho u_1 \\ 0 & 0 & \rho & 0 & \rho u_2 \\ 0 & 0 & 0 & \rho & \rho u_3 \\ 0 & 0 & 0 & 0 & \frac{1}{\gamma - 1} \end{bmatrix}$$

$$M^{-1^T} = \begin{bmatrix} 1 & -\frac{u_1}{\rho} & -\frac{u_2}{\rho} & -\frac{u_3}{\rho} & \frac{(\gamma - 1)u_i u_i}{2} \\ 0 & \frac{1}{\rho} & 0 & 0 & -(\gamma - 1)u_1 \\ 0 & 0 & \frac{1}{\rho} & 0 & -(\gamma - 1)u_2 \\ 0 & 0 & 0 & \frac{1}{\rho} & -(\gamma - 1)u_3 \\ 0 & 0 & 0 & 0 & \gamma - 1 \end{bmatrix}.$$

The conservative and primitive adjoint operators L and $\tilde{L}$ corresponding to the variations δw and $\delta \tilde{w}$ are then related by

$$\int_{\mathcal{D}} \delta w^T L \psi \, d\mathcal{D}_\xi = \int_{\mathcal{D}} \delta \tilde{w}^T \tilde{L} \psi \, d\mathcal{D}_\xi,$$

with

$$\tilde{L} = M^T L,$$

so that after determining the primitive adjoint operator by direct evaluation of the viscous portion of (22), the conservative operator may be obtained by the transformation $L = M^{-1^T} \tilde{L}$. Since the continuity equation contains no viscous terms, it makes no contribution to the viscous adjoint system. Therefore, the derivation proceeds by first examining the adjoint operators arising from the momentum equations.

Contributions from the Momentum Equations

In order to make use of the summation convention, it is convenient to set $\psi_{j+1} = \phi_j$ for $j = 1, 2, 3$. Then the contribution from the momentum equations is

$$\int_{\mathcal{B}} \phi_k \left(\delta S_{2j} \sigma_{kj} + S_{2j} \delta \sigma_{kj} \right) d\mathcal{B}_\xi$$

$$- \int_{\mathcal{D}} \frac{\partial \phi_k}{\partial \xi_i} \left(\delta S_{ij} \sigma_{kj} + S_{ij} \delta \sigma_{kj} \right) d\mathcal{D}_\xi. \quad (28)$$

The velocity derivatives in the viscous stresses can be expressed as

$$\frac{\partial u_i}{\partial x_j} = \frac{\partial u_i}{\partial \xi_l} \frac{\partial \xi_l}{\partial x_j} = \frac{S_{lj}}{J} \frac{\partial u_i}{\partial \xi_l}$$

with corresponding variations

$$\delta \frac{\partial u_i}{\partial x_j} = \left[\frac{S_{lj}}{J} \right]_I \frac{\partial}{\partial \xi_l} \delta u_i + \left[\frac{\partial u_i}{\partial \xi_l} \right]_{II} \delta \left(\frac{S_{lj}}{J} \right).$$

The variations in the stresses are then

$$\delta \sigma_{kj} = \left\{ \mu \left[\frac{S_{lj}}{J} \frac{\partial}{\partial \xi_l} \delta u_k + \frac{S_{lk}}{J} \frac{\partial}{\partial \xi_l} \delta u_j \right] \right.$$
$$\left. + \lambda \left[\delta_{jk} \frac{S_{lm}}{J} \frac{\partial}{\partial \xi_l} \delta u_m \right] \right\}_I$$
$$+ \left\{ \mu \left[\delta \left(\frac{S_{lj}}{J} \right) \frac{\partial u_k}{\partial \xi_l} + \delta \left(\frac{S_{lk}}{J} \right) \frac{\partial u_j}{\partial \xi_l} \right] \right.$$
$$\left. + \lambda \left[\delta_{jk} \delta \left(\frac{S_{lm}}{J} \right) \frac{\partial u_m}{\partial \xi_l} \right] \right\}_{II}.$$

As before, only those terms with subscript I, which contain variations of the flow variables, need be considered further in deriving the adjoint operator. The field contributions that contain δu_i in equation (28) appear as

$$- \int_{\mathcal{D}} \frac{\partial \phi_k}{\partial \xi_i} S_{ij} \left\{ \mu \left(\frac{S_{lj}}{J} \frac{\partial}{\partial \xi_l} \delta u_k + \frac{S_{lk}}{J} \frac{\partial}{\partial \xi_l} \delta u_j \right) \right.$$
$$\left. + \lambda \delta_{jk} \frac{S_{lm}}{J} \frac{\partial}{\partial \xi_l} \delta u_m \right\} d\mathcal{D}_\xi.$$

This may be integrated by parts to yield

$$\int_{\mathcal{D}} \delta u_k \frac{\partial}{\partial \xi_l} \left(S_{lj} S_{ij} \frac{\mu}{J} \frac{\partial \phi_k}{\partial \xi_i} \right) d\mathcal{D}_\xi$$

$$+ \quad \int_{\mathcal{D}} \delta u_j \frac{\partial}{\partial \xi_l} \left(S_{lk} S_{ij} \frac{\mu}{J} \frac{\partial \phi_k}{\partial \xi_i} \right) d\mathcal{D}_\xi$$

$$+ \quad \int_{\mathcal{D}} \delta u_m \frac{\partial}{\partial \xi_l} \left(S_{lm} S_{ij} \frac{\lambda \delta_{jk}}{J} \frac{\partial \phi_k}{\partial \xi_i} \right) d\mathcal{D}_\xi,$$

where the boundary integral has been eliminated by noting that $\delta u_i = 0$ on the solid boundary. By exchanging indices, the field integrals may be combined to produce

$$\int_{\mathcal{D}} \delta u_k \frac{\partial}{\partial \xi_l} S_{lj} \left\{ \mu \left(\frac{S_{ij}}{J} \frac{\partial \phi_k}{\partial \xi_i} + \frac{S_{ik}}{J} \frac{\partial \phi_j}{\partial \xi_i} \right) \right.$$
$$\left. + \lambda \delta_{jk} \frac{S_{im}}{J} \frac{\partial \phi_m}{\partial \xi_i} \right\} d\mathcal{D}_\xi,$$

which is further simplified by transforming the inner derivatives back to Cartesian coordinates

$$\int_{\mathcal{D}} \delta u_k \frac{\partial}{\partial \xi_l} S_{lj} \left\{ \mu \left(\frac{\partial \phi_k}{\partial x_j} + \frac{\partial \phi_j}{\partial x_k} \right) + \lambda \delta_{jk} \frac{\partial \phi_m}{\partial x_m} \right\} d\mathcal{D}_\xi. \tag{29}$$

The boundary contributions that contain δu_i in equation (28) may be simplified using the fact that

$$\frac{\partial}{\partial \xi_l} \delta u_i = 0 \quad \text{if} \quad l = 1, 3$$

on the boundary $\mathcal{B}$ so that they become

$$\int_{\mathcal{B}} \phi_k S_{2j} \left\{ \mu \left(\frac{S_{2j}}{J} \frac{\partial}{\partial \xi_2} \delta u_k + \frac{S_{2k}}{J} \frac{\partial}{\partial \xi_2} \delta u_j \right) \right.$$
$$\left. + \lambda \delta_{jk} \frac{S_{2m}}{J} \frac{\partial}{\partial \xi_2} \delta u_m \right\} d\mathcal{B}_\xi. \tag{30}$$

Together, (29) and (30) comprise the field and boundary contributions of the momentum equations to the viscous adjoint operator in primitive variables.

Contributions from the Energy Equation

In order to derive the contribution of the energy equation to the viscous adjoint terms it is convenient to set

$$\psi_5 = \theta, \quad Q_j = u_i \sigma_{ij} + \kappa \frac{\partial}{\partial x_j} \left(\frac{p}{\rho} \right),$$

where the temperature has been written in terms of pressure and density using (12). The contribution from the energy equation can then be written as

$$\int_{\mathcal{B}} \theta \left(\delta S_{2j} Q_j + S_{2j} \delta Q_j \right) d\mathcal{B}_\xi$$

$$- \quad \int_{\mathcal{D}} \frac{\partial \theta}{\partial \xi_i} \left(\delta S_{ij} Q_j + S_{ij} \delta Q_j \right) d\mathcal{D}_\xi. \tag{31}$$

The field contributions that contain $\delta u_i, \delta p$, and $\delta \rho$ in equation (31) appear as

$$- \int_{\mathcal{D}} \frac{\partial \theta}{\partial \xi_i} S_{ij} \delta Q_j \, d\mathcal{D}_\xi =$$
$$- \int_{\mathcal{D}} \frac{\partial \theta}{\partial \xi_i} S_{ij} \left\{ \delta u_k \sigma_{kj} + u_k \delta \sigma_{kj} \right.$$
$$\left. + \kappa \frac{S_{lj}}{J} \frac{\partial}{\partial \xi_l} \left(\frac{\delta p}{\rho} - \frac{p}{\rho} \frac{\delta \rho}{\rho} \right) \right\} d\mathcal{D}_\xi. \tag{32}$$

The term involving $\delta \sigma_{kj}$ may be integrated by parts to produce

$$\int_{\mathcal{D}} \delta u_k \frac{\partial}{\partial \xi_l} S_{lj} \left\{ \mu \left(u_k \frac{\partial \theta}{\partial x_j} + u_j \frac{\partial \theta}{\partial x_k} \right) \right.$$
$$\left. + \lambda \delta_{jk} u_m \frac{\partial \theta}{\partial x_m} \right\} d\mathcal{D}_\xi, \tag{33}$$

where the conditions $u_i = \delta u_i = 0$ are used to eliminate the boundary integral on $\mathcal{B}$. Notice that the other term in (32) that involves δu_k need not be integrated by parts and is merely carried on as

$$- \int_{\mathcal{D}} \delta u_k \sigma_{kj} S_{ij} \frac{\partial \theta}{\partial \xi_i} d\mathcal{D}_\xi \tag{34}$$

The terms in expression (32) that involve δp and $\delta \rho$ may also be integrated by parts to produce both a field and a boundary integral. The field integral becomes

$$\int_{\mathcal{D}} \left(\frac{\delta p}{\rho} - \frac{p}{\rho} \frac{\delta \rho}{\rho} \right) \frac{\partial}{\partial \xi_l} \left(S_{lj} S_{ij} \frac{\kappa}{J} \frac{\partial \theta}{\partial \xi_i} \right) d\mathcal{D}_\xi$$

which may be simplified by transforming the inner derivative to Cartesian coordinates

$$\int_{\mathcal{D}} \left(\frac{\delta p}{\rho} - \frac{p}{\rho} \frac{\delta \rho}{\rho} \right) \frac{\partial}{\partial \xi_l} \left(S_{lj} \kappa \frac{\partial \theta}{\partial x_j} \right) d\mathcal{D}_\xi. \tag{35}$$

The boundary integral becomes

$$\int_{\mathcal{B}} \kappa \left(\frac{\delta p}{\rho} - \frac{p}{\rho} \frac{\delta \rho}{\rho} \right) \frac{S_{2j} S_{ij}}{J} \frac{\partial \theta}{\partial \xi_i} d\mathcal{B}_\xi. \tag{36}$$

This can be simplified by transforming the inner derivative to Cartesian coordinates

$$\int_{\mathcal{B}} \kappa \left(\frac{\delta p}{\rho} - \frac{p}{\rho} \frac{\delta \rho}{\rho} \right) \frac{S_{2j}}{J} \frac{\partial \theta}{\partial x_j} d\mathcal{B}_\xi, \tag{37}$$

and identifying the normal derivative at the wall

$$\frac{\partial}{\partial n} = S_{2j} \frac{\partial}{\partial x_j}, \tag{38}$$

and the variation in temperature

$$\delta T = \frac{1}{R} \left(\frac{\delta p}{\rho} - \frac{p}{\rho} \frac{\delta \rho}{\rho} \right),$$

to produce the boundary contribution

$$\int_{\mathcal{B}} k\,\delta T \frac{\partial \theta}{\partial n}\, d\mathcal{B}_\xi. \qquad (39)$$

This term vanishes if T is constant on the wall but persists if the wall is adiabatic.

There is also a boundary contribution left over from the first integration by parts (31) which has the form

$$\int_{\mathcal{B}} \theta\,\delta\left(S_{2j}Q_j\right) d\mathcal{B}_\xi, \qquad (40)$$

where

$$Q_j = k\frac{\partial T}{\partial x_j},$$

since $u_i = 0$. Notice that for future convenience in discussing the adjoint boundary conditions resulting from the energy equation, both the δw and δS terms corresponding to subscript classes I and II are considered simultaneously. If the wall is adiabatic

$$\frac{\partial T}{\partial n} = 0,$$

so that using (38),

$$\delta\left(S_{2j}Q_j\right) = 0,$$

and both the δw and δS boundary contributions vanish.

On the other hand, if T is constant $\frac{\partial T}{\partial \xi_l} = 0$ for $l = 1,3$, so that

$$Q_j = k\frac{\partial T}{\partial x_j} = k\left(\frac{S_{lj}}{J}\frac{\partial T}{\partial \xi_l}\right) = k\left(\frac{S_{2j}}{J}\frac{\partial T}{\partial \xi_2}\right).$$

Thus, the boundary integral (40) becomes

$$\int_{\mathcal{B}} k\theta\left\{\frac{S_{2j}{}^2}{J}\frac{\partial}{\partial \xi_2}\delta T + \delta\left(\frac{S_{2j}{}^2}{J}\right)\frac{\partial T}{\partial \xi_2}\right\} d\mathcal{B}_\xi. \quad (41)$$

Therefore, for constant T, the first term corresponding to variations in the flow field contributes to the adjoint boundary operator and the second set of terms corresponding to metric variations contribute to the cost function gradient.

All together, the contributions from the energy equation to the viscous adjoint operator are the three field terms (33), (34) and (35), and either of two boundary contributions (39) or (41), depending on whether the wall is adiabatic or has constant temperature.

The Viscous Adjoint Field Operator

Collecting together the contributions from the momentum and energy equations, the viscous adjoint operator in primitive variables can be expressed as

$$
\begin{aligned}
(\tilde{L}\psi)_1 &= -\frac{p}{\rho^2}\frac{\partial}{\partial \xi_l}\left(S_{lj}\kappa\frac{\partial \theta}{\partial x_j}\right) \\
(\tilde{L}\psi)_{i+1} &= \frac{\partial}{\partial \xi_l}\left\{S_{lj}\left[\mu\left(\frac{\partial \phi_i}{\partial x_j} + \frac{\partial \phi_j}{\partial x_i}\right) + \lambda\delta_{ij}\frac{\partial \phi_k}{\partial x_k}\right]\right\} \\
&+ \frac{\partial}{\partial \xi_l}\left\{S_{lj}\left[\mu\left(u_i\frac{\partial \theta}{\partial x_j} + u_j\frac{\partial \theta}{\partial x_i}\right) + \lambda\delta_{ij}u_k\frac{\partial \theta}{\partial x_k}\right]\right\} \\
&- \sigma_{ij}S_{lj}\frac{\partial \theta}{\partial \xi_l} \qquad \text{for} \quad i = 1,2,3 \\
(\tilde{L}\psi)_5 &= \frac{1}{\rho}\frac{\partial}{\partial \xi_l}\left(S_{lj}\kappa\frac{\partial \theta}{\partial x_j}\right).
\end{aligned}
$$

The conservative viscous adjoint operator may now be obtained by the transformation

$$L = M^{-1T}\tilde{L}.$$

7 Viscous Adjoint Boundary Conditions

It was recognized in Section 4 that the boundary conditions satisfied by the flow equations restrict the form of the performance measure that may be chosen for the cost function. There must be a direct correspondence between the flow variables for which variations appear in the variation of the cost function, and those variables for which variations appear in the boundary terms arising during the derivation of the adjoint field equations. Otherwise it would be impossible to eliminate the dependence of δI on δw through proper specification of the adjoint boundary condition. As in the derivation of the field equations, it proves convenient to consider the contributions from the momentum equations and the energy equation separately.

Boundary Conditions Arising from the Momentum Equations

The boundary term that arises from the momentum equations including both the δw and δS components (28) takes the form

$$\int_{\mathcal{B}} \phi_k\,\delta\left(S_{2j}\sigma_{kj}\right) d\mathcal{B}_\xi.$$

Replacing the metric term with the corresponding local face area S_2 and unit normal n_j defined by

$$|S_2| = \sqrt{S_{2j}S_{2j}}, \quad n_j = \frac{S_{2j}}{|S_2|}$$

then leads to

$$\int_{\mathcal{B}} \phi_k \delta \left(|S_2| \, n_j \sigma_{kj} \right) d\mathcal{B}_\xi.$$

Defining the components of the surface stress as

$$\tau_k = n_j \sigma_{kj}$$

and the physical surface element

$$dS = |S_2| \, d\mathcal{B}_\xi,$$

the integral may then be split into two components

$$\int_{\mathcal{B}} \phi_k \tau_k \, |\delta S_2| \, d\mathcal{B}_\xi + \int_{\mathcal{B}} \phi_k \delta \tau_k dS, \qquad (42)$$

where only the second term contains variations in the flow variables and must consequently cancel the δw terms arising in the cost function. The first term will appear in the expression for the gradient.

A general expression for the cost function that allows cancellation with terms containing $\delta \tau_k$ has the form

$$I = \int_{\mathcal{B}} \mathcal{N}(\tau) dS, \qquad (43)$$

corresponding to a variation

$$\delta I = \int_{\mathcal{B}} \frac{\partial \mathcal{N}}{\partial \tau_k} \delta \tau_k dS,$$

for which cancellation is achieved by the adjoint boundary condition

$$\phi_k = \frac{\partial \mathcal{N}}{\partial \tau_k}.$$

Natural choices for $\mathcal{N}$ arise from force optimization and as measures of the deviation of the surface stresses from desired target values.

For viscous force optimization, the cost function should measure friction drag. The friction force in the x_i direction is

$$CD_{fi} = \int_{\mathcal{B}} \sigma_{ij} dS_j = \int_{\mathcal{B}} S_{2j} \sigma_{ij} d\mathcal{B}_\xi$$

so that the force in a direction with cosines n_i has the form

$$C_{nf} = \int_{\mathcal{B}} n_i S_{2j} \sigma_{ij} d\mathcal{B}_\xi.$$

Expressed in terms of the surface stress τ_i, this corresponds to

$$C_{nf} = \int_{\mathcal{B}} n_i \tau_i dS,$$

so that basing the cost function (43) on this quantity gives

$$\mathcal{N} = n_i \tau_i.$$

Cancellation with the flow variation terms in equation (42) therefore mandates the adjoint boundary condition

$$\phi_k = n_k.$$

Note that this choice of boundary condition also eliminates the first term in equation (42) so that it need not be included in the gradient calculation.

In the inverse design case, where the cost function is intended to measure the deviation of the surface stresses from some desired target values, a suitable definition is

$$\mathcal{N}(\tau) = \frac{1}{2} a_{lk} \left(\tau_l - \tau_{dl} \right) \left(\tau_k - \tau_{dk} \right),$$

where τ_d is the desired surface stress, including the contribution of the pressure, and the coefficients a_{lk} define a weighting matrix. For cancellation

$$\phi_k \delta \tau_k = a_{lk} \left(\tau_l - \tau_{dl} \right) \delta \tau_k.$$

This is satisfied by the boundary condition

$$\phi_k = a_{lk} \left(\tau_l - \tau_{dl} \right). \qquad (44)$$

Assuming arbitrary variations in $\delta \tau_k$, this condition is also necessary.

In order to control the surface pressure and normal stress one can measure the difference

$$n_j \left\{ \sigma_{kj} + \delta_{kj} \left(p - p_d \right) \right\},$$

where p_d is the desired pressure. The normal component is then

$$\tau_n = n_k n_j \sigma_{kj} + p - p_d,$$

so that the measure becomes

$$\begin{aligned} \mathcal{N}(\tau) &= \frac{1}{2} \tau_n^2 \\ &= \frac{1}{2} n_l n_m n_k n_j \left\{ \sigma_{lm} + \delta_{lm} \left(p - p_d \right) \right\} \\ &\quad \cdot \left\{ \sigma_{kj} + \delta_{kj} \left(p - p_d \right) \right\}. \end{aligned}$$

This corresponds to setting

$$a_{lk} = n_l n_k$$

in equation (44). Defining the viscous normal stress as

$$\tau_{vn} = n_k n_j \sigma_{kj},$$

the measure can be expanded as

$$\begin{aligned} \mathcal{N}(\tau) &= \frac{1}{2} n_l n_m n_k n_j \sigma_{lm} \sigma_{kj} \\ &\quad + \frac{1}{2} \left(n_k n_j \sigma_{kj} + n_l n_m \sigma_{lm} \right) \left(p - p_d \right) + \frac{1}{2} \left(p - p_d \right)^2 \\ &= \frac{1}{2} \tau_{vn}^2 + \tau_{vn} \left(p - p_d \right) + \frac{1}{2} \left(p - p_d \right)^2. \end{aligned}$$

For cancellation of the boundary terms

$$\phi_k \left(n_j \delta \sigma_{kj} + n_k \delta p \right) =$$
$$\left\{ n_l n_m \sigma_{lm} + n_l^2 \left(p - p_d \right) \right\} n_k \left(n_j \delta \sigma_{kj} + n_k \delta p \right)$$

leading to the boundary condition

$$\phi_k = n_k \left(\tau_{vn} + p - p_d \right).$$

In the case of high Reynolds number, this is well approximated by the equations

$$\phi_k = n_k \left(p - p_d \right), \qquad (45)$$

which should be compared with the single scalar equation derived for the inviscid boundary condition (27). In the case of an inviscid flow, choosing

$$\mathcal{N}(\tau) = \frac{1}{2} \left(p - p_d \right)^2$$

requires

$$\phi_k n_k \delta p = \left(p - p_d \right) n_k^2 \delta p = \left(p - p_d \right) \delta p$$

which is satisfied by equation (45), but which represents an overspecification of the boundary condition since only the single condition (27) need be specified to ensure cancellation.

Boundary Conditions Arising from the Energy Equation

The form of the boundary terms arising from the energy equation depends on the choice of temperature boundary condition at the wall. For the adiabatic case, the boundary contribution is (39)

$$\int_{\mathcal{B}} k \delta T \frac{\partial \theta}{\partial n} d\mathcal{B}_\xi,$$

while for the constant temperature case the boundary term is (41). One possibility is to introduce a contribution into the cost function which depends on T or $\frac{\partial T}{\partial n}$ so that the appropriate cancellation would occur. Since there is little physical intuition to guide the choice of such a cost function for aerodynamic design, a more natural solution is to set

$$\theta = 0$$

in the constant temperature case or

$$\frac{\partial \theta}{\partial n} = 0$$

in the adiabatic case. Note that in the constant temperature case, this choice of θ on the boundary would also eliminate the boundary metric variation terms in (40).

8 Implementation of Navier-Stokes Design

The design procedures can be summarized as follows:

1. Solve the flow equations for ρ, u_1, u_2, u_3, p.

2. Solve the adjoint equations for ψ subject to appropriate boundary conditions.

3. Evaluate $\mathcal{G}$.

4. Project $\mathcal{G}$ into an allowable subspace that satisfies any geometric constraints.

5. Update the shape based on the direction of steepest descent.

6. Return to 1 until convergence is reached.

Practical implementation of the viscous design method relies heavily upon fast and accurate solvers for both the state (w) and co-state (ψ) systems. This work uses well-validated software for the solution of the Euler and Navier-Stokes equations developed over the course of many years [23, 24, 25].

For inverse design the lift is fixed by the target pressure. In drag minimization it is also appropriate to fix the lift coefficient, because the induced drag is a major fraction of the total drag, and this could be reduced simply by reducing the lift. Therefore the angle of attack is adjusted during the flow solution to force a specified lift coefficient to be attained, and the influence of variations of the angle of attack is included in the calculation of the gradient. The vortex drag also depends on the span loading, which may be constrained by other considerations such as structural loading or buffet onset. Consequently, the option is provided to force the span loading by adjusting the twist distribution as well as the angle of attack during the flow solution.

Discretization

Both the flow and the adjoint equations are discretized using a semi-discrete cell-centered finite volume scheme. The convective fluxes across cell interfaces are represented by simple arithmetic averages of the fluxes computed using values from the cells on either side of the face, augmented by artificial diffusive terms to prevent numerical oscillations in the vicinity of shock waves. Continuing to use the summation convention for repeated indices, the numerical convective flux across the interface between cells A and B in a three dimensional mesh has the form

$$h_{AB} = \frac{1}{2} S_{AB_j} \left(f_{A_j} + f_{B_j} \right) - d_{AB},$$

where S_{AB_j} is the component of the face area in the jth Cartesian coordinate direction, (f_{A_j}) and (f_{B_j}) denote the flux f_j as defined by equation (12) and d_{AB} is the diffusive term. Variations of the computer program provide options for alternate constructions of the diffusive flux.

The simplest option implements the Jameson-Schmidt-Turkel scheme [23, 26], using scalar diffusive terms of the form

$$d_{AB} = \epsilon^{(2)} \Delta w - \epsilon^{(4)} \left(\Delta w^+ - 2\Delta w + \Delta w^- \right),$$

where

$$\Delta w = w_B - w_A$$

and Δw^+ and Δw^- are the same differences across the adjacent cell interfaces behind cell A and beyond cell B in the AB direction. By making the coefficient $\epsilon^{(2)}$ depend on a switch proportional to the undivided second difference of a flow quantity such as the pressure or entropy, the diffusive flux becomes a third order quantity, proportional to the cube of the mesh width in regions where the solution is smooth. Oscillations are suppressed near a shock wave because $\epsilon^{(2)}$ becomes of order unity, while $\epsilon^{(4)}$ is reduced to zero by the same switch. For a scalar conservation law, it is shown in reference [26] that $\epsilon^{(2)}$ and $\epsilon^{(4)}$ can be constructed to make the scheme satisfy the local extremum diminishing (LED) principle that local maxima cannot increase while local minima cannot decrease.

The second option applies the same construction to local characteristic variables. There are derived from the eigenvectors of the Jacobian matrix A_{AB} which exactly satisfies the relation

$$A_{AB} \left(w_B - w_A \right) = S_{AB_j} \left(f_{B_j} - f_{A_j} \right).$$

This corresponds to the definition of Roe [27]. The resulting scheme is LED in the characteristic variables. The third option implements the H-CUSP scheme proposed by Jameson [28] which combines differences $f_B - f_A$ and $w_B - w_A$ in a manner such that stationary shock waves can be captured with a single interior point in the discrete solution. This scheme minimizes the numerical diffusion as the velocity approaches zero in the boundary layer, and has therefore been preferred for viscous calculations in this work.

Similar artificial diffusive terms are introduced in the discretization of the adjoint equation, but with the opposite sign because the wave directions are reversed in the adjoint equation. Satisfactory results have been obtained using scalar diffusion in the adjoint equation while characteristic or H-CUSP constructions are used in the flow solution.

The discretization of the viscous terms of the Navier Stokes equations requires the evaluation of
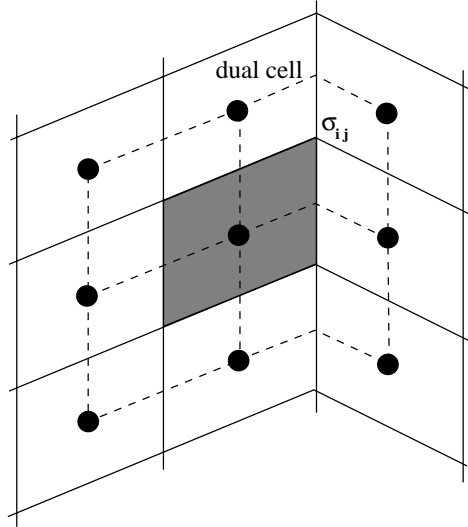
Figure 1: Cell-centered scheme. σ_{ij} evaluated at vertices of the primary mesh

the velocity derivatives $\frac{\partial u_i}{\partial x_j}$ in order to calculate the viscous stress tensor σ_{ij} defined in equation (11). These are most conveniently evaluated at the cell vertices of the primary mesh by introducing a dual mesh which connects the cell centers of the primary mesh, as depicted in Figure (1). According to the Gauss formula for a control volume V with boundary S

$$\int_V \frac{\partial v_i}{\partial x_j} dv = \int_S u_i n_j dS$$

where n_j is the outward normal. Applied to the dual cells this yields the estimate

$$\frac{\partial v_i}{\partial x_j} = \frac{1}{\text{vol}} \sum_{\text{faces}} \bar{u}_i n_j S$$

where S is the area of a face, and $\bar{u}_i$ is an estimate of the average of u_i over that face. In order to determine the viscous flux balance of each primary cell, the viscous flux across each of its faces is then calculated from the average of the viscous stress tensor at the four vertices connected by that face. This leads to a compact scheme with a stencil connecting each cell to its 26 nearest neighbors.

The semi-discrete schemes for both the flow and the adjoint equations are both advanced to steady state by a multi-stage time stepping scheme. This is a generalized Runge-Kutta scheme in which the convective and diffusive terms are treated differently to enlarge the stability region [26, 29]. Convergence to a steady state is accelerated by residual averaging and a multi-grid procedure [30]. These algorithms have been implemented both for single

and multiblock meshes and for operation on parallel computers with message passing using the MPI (Message Passing Interface) protocol [8, 31, 32].

In this work, the adjoint and flow equations are discretized separately. The alternative approach of deriving the discrete adjoint equations directly from the discrete flow equations yields another possible discretization of the adjoint partial differential equation which is more complex. If the resulting equations were solved exactly, they could provide the exact gradient of the inexact cost function which results from the discretization of the flow equations. On the other hand, any consistent discretization of the adjoint partial differential equation will yield the exact gradient as the mesh is refined, and separate discretization has proved to work perfectly well in practice. It should also be noted that the discrete gradient includes both mesh effects and numerical errors such as spurious entropy production which may not reflect the true cost function of the continuous problem.

Mesh Generation and Geometry Control

Meshes for both viscous optimization and for the treatment of complex configurations are externally generated in order to allow for their inspection and careful quality control. Single block meshes with a C-H topology have been used for viscous optimization of wing-body combinations, while multiblock meshes have been generated for complex configurations using GRIDGEN [33]. In either case geometry modifications are accommodated by a grid perturbation scheme. For viscous wing-body design using single block meshes, the wing surface mesh points themselves are taken as the design variables. A simple mesh perturbation scheme is then used, in which the mesh points lying on a mesh line projecting out from the wing surface are all shifted in the same sense as the surface mesh point, with a decay factor proportional to the arc length along the mesh line. The resulting perturbation in the face areas of the neighboring cells are then included in the gradient calculation. For complex configurations the geometry is controlled by superposition of analytic "bump" functions defined over the surfaces which are to be modified. The grid is then perturbed to conform to modifications of the surface shape by the WARP3D and WARP-MB algorithms described in [31].

Optimization

Two main search procedures have been used in our applications to date. The first is a simple descent method in which small steps are taken in the negative gradient direction. Let $\mathcal{F}$ represent the design variable, and $\mathcal{G}$ the gradient. Then the iteration

$$\delta \mathcal{F} = -\lambda \mathcal{G}$$

can be regarded as simulating the time dependent process

$$\frac{d\mathcal{F}}{dt} = -\mathcal{G}$$

where λ is the time step Δt. Let A be the Hessian matrix with elements

$$A_{ij} = \frac{\partial \mathcal{G}_i}{\partial \mathcal{F}_j} = \frac{\partial^2 I}{\partial \mathcal{F}_i \partial \mathcal{F}_j}.$$

Suppose that a locally minimum value of the cost function $I^* = I(\mathcal{F}^*)$ is attained when $\mathcal{F} = \mathcal{F}^*$. Then the gradient $\mathcal{G}^* = \mathcal{G}(\mathcal{F}^*)$ must be zero, while the Hessian matrix $A^* = A(\mathcal{F}^*)$ must be positive definite. Since $\mathcal{G}^*$ is zero, the cost function can be expanded as a Taylor series in the neighborhood of $\mathcal{F}^*$ with the form

$$I(\mathcal{F}) = I^* + \frac{1}{2} \left(\mathcal{F} - \mathcal{F}^* \right) A \left(\mathcal{F} - \mathcal{F}^* \right) + \ldots$$

Correspondingly,

$$\mathcal{G}(\mathcal{F}) = A \left(\mathcal{F} - \mathcal{F}^* \right) + \ldots$$

As $\mathcal{F}$ approaches $\mathcal{F}^*$, the leading terms become dominant. Then, setting $\hat{\mathcal{F}} = (\mathcal{F} - \mathcal{F}^*)$, the search process approximates

$$\frac{d\hat{\mathcal{F}}}{dt} = -A^* \hat{\mathcal{F}}.$$

Also, since A^* is positive definite it can be expanded as

$$A^* = R M R^T,$$

where M is a diagonal matrix containing the eigenvalues of A^*, and

$$R R^T = R^T R = I.$$

Setting

$$v = R^T \hat{\mathcal{F}},$$

the search process can be represented as

$$\frac{dv}{dt} = -M v.$$

The stability region for the simple forward Euler stepping scheme is a unit circle centered at -1 on the negative real axis. Thus for stability we must choose

$$\mu_{\max} \Delta t = \mu_{\max} \lambda < 2,$$

while the asymptotic decay rate, given by the smallest eigenvalue, is proportional to

$$e^{-\mu_{\min}t}.$$

In order to make sure that each new shape in the optimization sequence remains smooth, it proves essential to smooth the gradient and to replace $\mathcal{G}$ by its smoothed value $\bar{\mathcal{G}}$ in the descent process. This also acts as a preconditioner which allows the use of much larger steps. To apply smoothing in the ξ_1 direction, for example, the smoothed gradient $\bar{\mathcal{G}}$ ma be calculated from a discrete approximation to

$$\bar{\mathcal{G}} - \frac{\partial}{\partial\xi_1}\epsilon\frac{\partial}{\partial\xi_1}\bar{\mathcal{G}} = \mathcal{G}$$

where ϵ is the smoothing parameter. If one sets $\delta\mathcal{F} = -\lambda\bar{\mathcal{G}}$, then, assuming the modification is applied on the surface $\xi_2 = $ constant, the first order change in the cost function is

$$\begin{aligned}\delta I &= -\iint \mathcal{G}\delta\mathcal{F}\,d\xi_1 d\xi_3 \\ &= -\lambda\iint\left(\bar{\mathcal{G}} - \frac{\partial}{\partial\xi_1}\epsilon\frac{\partial\bar{\mathcal{G}}}{\partial\xi_1}\right)\bar{\mathcal{G}}\,d\xi_1 d\xi_3 \\ &= -\lambda\iint\left(\bar{\mathcal{G}}^2 + \epsilon\left(\frac{\partial\bar{\mathcal{G}}}{\partial\xi_1}\right)^2\right)d\xi_1 d\xi_3 \\ &< 0,\end{aligned}$$

assuring an improvement if λ is sufficiently small and positive, unless the process has already reached a stationary point at which $\mathcal{G} = 0$.

It turns out that this approach is tolerant to the use of approximate values of the gradient, so that neither the flow solution nor the adjoint solution need be fully converged before making a shape change. This results in very large savings in the computational cost. For inviscid optimization it is necessary to use only 15 multigrid cycles for the flow solution and the adjoint solution in each design iteration. For viscous optimization, about 100 multigrid cycles are needed. This is partly because convergence of the lift coefficient is much slower, so about 20 iterations must be made before each adjustment of the angle of attack to force the target lift coefficient.

Our second main search procedure incorporates a quasi-Newton method for general constrained optimization. In this class of methods the step is defined as

$$\delta\mathcal{F} = -\lambda P\mathcal{G},$$

where P is a preconditioner for the search. An ideal choice is $P = A^{*-1}$, so that the corresponding time dependent process reduces to

$$\frac{d\hat{\mathcal{F}}}{dt} = -\hat{\mathcal{F}},$$

for which all the eigenvalues are equal to unity, and $\hat{\mathcal{F}}$ is reduced to zero in one time step by the choice $\Delta t = 1$ if the Hessian, A, is constant. The full Newton method takes $P = A^{-1}$, requiring the evaluation of the Hessian matrix, A, at each step. It corresponds to the use of the Newton-Raphson method to solve the non-linear equation $\mathcal{G} = 0$. Quasi-Newton methods estimate A^* from the change in the gradient during the search process. This requires accurate estimates of the gradient at each time step. In order to obtain these, both the flow solution and the adjoint equation must be fully converged. Most quasi-Newton methods also require a line search in each search direction, for which the flow equations and cost function must be accurately evaluated several times. They have proven quite robust for aerodynamic optimization [34].

In the applications to complex configurations presented below the optimization was carried out using the existing, well validated software NPSOL. This software, which implements a quasi-Newton method for optimization with both linear and non-linear constraints, has proved very reliable but is generally more expensive than the simple search method with smoothing.

9 Industrial Experience and Results

The methods described in this paper have been quite thoroughly tested in industrial applications in which they were used as a tool for aerodynamic design. They have proved useful both in inverse mode to find shapes that would produce desired pressure distributions, and for direct minimization of the drag. They have been applied both to well understood configurations that have gradually evolved through incremental improvements guided by wind tunnel tests and computational simulation, and to new concepts for which there is a limited knowledge base. In either case they have enabled engineers to produce improved designs.

Substantial improvements are usually obtained with $20 - 200$ design cycles, depending on the difficulty of the case. One concern is the possibility of getting trapped in a local minimum. In practice this has not proved to be a source of difficulty. In inverse mode, it often proves possible to come very close to realizing the target pressure distribution, thus effectively demonstrating convergence. In drag minimization, the result of the optimization is usually a shock-free wing. If one considers drag minimization of airfoils in two-dimensional inviscid transonic flow, it can be seen that every shock-free airfoil produces zero drag, and thus optimization

based solely on drag has a highly non-unique solution. Different shock-free airfoils can be obtained by starting from different initial profiles. One may also influence the character of the final design by blending a target pressure distribution with the drag in the definition of the cost function.

Similar considerations apply to three-dimensional wing design in viscous transonic flow. Since the vortex drag can be reduced simply by reducing the lift, the lift coefficient must be fixed for a meaningful drag minimization. A typical wing of a transport aircraft is designed for a lift coefficient in the range of 0.4 to 0.6. The total wing drag may be broken down into vortex drag, drag due to viscous effects, and shock drag. The vortex drag coefficient is typically in the range of 0.0100 (100 counts), while the friction drag coefficient is in the range of 45 counts, and the shock drag at a Mach number just before the onset of severe drag rise is of the order of 15 counts. With a fixed span, typically dictated by structural limits or a constraint imposed by airport gates, the vortex drag is entirely a function of span loading, and is minimized by an elliptic loading unless winglets are added. Transport aircraft usually have highly tapered wings with very large root chords to accommodate retraction of the undercarriage. An elliptic loading may lead to excessively large section lift coefficients on the outboard wing, leading to premature shock stall or buffet when the load is increased. The structure weight is also reduced by a more inboard loading which reduces the root bending moment. Thus the choice of span loading is influenced by other considerations. The skin friction of transport aircraft is typically very close to flat plate skin friction in turbulent flow, and is very insensitive to section variations. An exception to this is the case of smaller executive jet aircraft, for which the Reynolds number may be small enough to allow a significant run of laminar flow if the suction peak of the pressure distribution is moved back on the section. This leaves the shock drag as the primary target for wing section optimization. This is reduced to zero if the wing is shock-free, leaving no room for further improvement. Thus the attainment of a shock-free flow is a demonstration of a successful drag minimization. In practice range is maximized by maximizing $M \frac{L}{D}$, and this is likely to be increased by increasing the lift coefficient to the point where a weak shock appears. One may also use optimization to find the maximum Mach number at which the shock drag can be eliminated or significantly reduced for a wing with a given sweepback angle and thickness. Alternatively one may try to find the largest wing thickness or the minimum sweepback angle for which the shock drag can

be eliminated at a given Mach number. This can yield both savings in structure weight and increased fuel volume . If there is no fixed limit for the wing span, such as a gate constraint, increased thickness can be used to allow an increase in aspect ratio for a wing of equal weight, in turn leading to a reduction in vortex drag. Since the vortex drag is usually the largest component of the total wing drag, this is probably the most effective design strategy, and it may pay to increase the wing thickness to the point where the optimized section produces a weak shock wave rather than a shock-free flow [22].

The first major industrial application of an adjoint based aerodynamic optimization method was the wing design of the Beech Premier [35] in 1995. The method was successfully used in inverse mode as a tool to obtain pressure distributions favorable to the maintenance of natural laminar flow over a range of cruise Mach numbers. Wing contours were obtained which yielded the desired pressure distribution in the presence of closely coupled engine nacelles on the fuselage above the wing trailing edge.

During 1996 some preliminary studies indicated that the wings of both the McDonnell Douglas MD-11 and the Boeing 747-200 could be made shock-free in a representative cruise condition by using very small shape modifications, with consequent drag savings which could amount to several percent of the total drag. This led to a decision to evaluate adjoint-based design methods in the design of the McDonnell Douglas MDXX during the summer and fall of 1996. In initial studies wing redesigns were carried out for inviscid transonic flow modelled by the Euler equations. A redesign to minimize the drag at a specified lift and Mach number required about 40 design cycles, which could be completed overnight on a workstation.

Three main lessons were drawn from these initial studies: (i) the fuselage effect is to large to be ignored and must be included in the optimization, (ii) single-point designs could be too sensitive to small variations in the flight condition, typically producing a shock-free flow at the design point with a tendency to break up into a severe double shock pattern below the design point, and (iii) the shape changes necessary to optimize a wing in transonic flow are smaller than the boundary layer displacement thickness, with the consequence that viscous effects must be included in the final design.

In order to meet the first two of these considerations, the second phase of the study was concentrated on the optimization of wing-body combinations with multiple design points. These were still performed with inviscid flow to reduce computational cost and allow for fast turnaround. It was found that comparatively insensitive designs

could be obtained by minimizing the drag at a fixed Mach number for three fairly closely spaced lift coefficients such as 0.5, 0.525, and 0.55, or alternatively three nearby Mach numbers with a fixed lift coefficient.

The third phase of the project was focused on the design with viscous effects using as a starting point wings which resulted from multipoint inviscid optimization. While the full viscous adjoint method was still under development, it was found that useful improvements could be realized, particularly in inverse mode, using the inviscid result to provide the target pressure, by coupling an inviscid adjoint solver to a viscous flow solver. Computer costs are many times larger, both because finer meshes are needed to resolve the boundary layer, and because more iterations are needed in the flow and adjoint solutions. In order to force the specified lift coefficient the number of iterations in each flow solution had to be increased from 15 to 100. To achieve overnight turnaround a fully parallel implementation of the software had to be developed. Finally it was found that in order to produce sufficiently accurate results, the number of mesh points had to be increased to about 1.8 million. In the final phase of this project it was planned to carry out a propulsion integration study using the multiblock versions of the software. This study was not completed due to the cancellation of the entire MDXX project.

During the summer of 1997, adjoint methods were again used to assist the McDonnell Douglas Blended Wing-Body project. By this time the viscous adjoint method was well developed, and it was found that it was needed to achieve truly smooth shock-free solutions. With an inviscid adjoint solver coupled to a viscous flow solver some improvements could be made, but the shocks could not be entirely eliminated.

The next subsection shows a wing design using the full viscous adjoint method in its current form, implemented in the computer program SYN107. The remaining subsections present results of optimizations for complete configurations in inviscid transonic and supersonic flow using the multiblock parallel design program, SYN107-MB.

Transonic Viscous Wing-Body Design

A typical result of drag minimization in transonic viscous flow is presented below. This calculation is a redesign of a wing using the viscous adjoint optimization method with a Baldwin-Lomax turbulence model. The initial wing is similar to one produced during the MDXX design studies. Figures 2-4 show the result of the wing-body redesign

on a C-H mesh with $288 \times 96 \times 64$ cells. The wing has sweep back of about 38 degrees at the 1/4 chord. A total of 44 iterations of the viscous optimization procedure resulted in a shock-free wing at a cruise design point of Mach 0.86, with a lift coefficient of 0.61 for the wing-body combination at a Reynolds number of 101 million based on the root chord. Using 48 processors of an SGI Origin2000 parallel computer, each design iteration takes about 22 minutes so that overnight turnaround for such a calculation is possible. Figure 2 compares the pressure distribution of the final design with that of the initial wing. The final wing is quite thick, with a thickness to chord ratio of about 14 percent at the root and 9 percent at the tip. The optimization was performed with a constraint that the section modifications were not allowed to decrease the thickness anywhere. The design offers excellent performance at the nominal cruise point. A drag reduction of 2.2 counts was achieved from the initial wing which had itself been derived by inviscid optimization. Figures 3 and 4 show the results of a Mach number sweep to determine the drag rise. The drag coefficients shown in the figures represent the total wing drag including shock, vortex, and skin friction contributions. It can be seen that a double shock pattern forms below the design point, while there is actually a slight increase in the drag coefficient at Mach 0.85. The tendency to produce double shocks below the design point is typical of supercritical wings. This wing has a low drag coefficient, however, over a wide range of conditions. Above the design point a single shock forms and strengthens as the Mach number increases, a behavior typical in transonic flow.

Transonic Multipoint Constrained Aircraft Design

As a first example of the automatic design capability for complex configurations, a typical business jet configuration is chosen for a multipoint drag minimization run. The objective of the design is to alter the geometry of the wing in order to minimize the configuration inviscid drag at three different flight conditions simultaneously. Realistic geometric spar thickness constraints are enforced. The geometry chosen for this analysis is a full configuration business jet composed of wing, fuselage, pylon, nacelle, and empennage. The inviscid multiblock mesh around this configuration follows a general C-O topology with special blocking to capture the geometric details of the nacelles, pylons and empennage. A total of 240 point-to-point matched blocks with $4,157,440$ cells (including halos) are used to grid the complete configuration. This mesh

allows the use of 4 multigrid levels obtained through recursive coarsening of the initial fine mesh. The upstream, downstream, upper and lower far field boundaries are located at an approximate distance of 15 wing semispans, while the far field boundary beyond the wing tip is located at a distance approximately equal to 5 semispans. An engineering-accuracy solution (with a decrease of 4 orders of magnitude in the average density residual) can be obtained in 100 multigrid cycles. This kind of solution can be routinely accomplished in under 20 minutes of wall clock time using 32 processors of an SGI Origin2000 computer.

The initial configuration was designed for Mach $= 0.8$ and $C_L = 0.3$. The three operating points chosen for this design are Mach $= 0.81$ with $C_L = 0.35$, Mach $= 0.82$ with $C_L = 0.30$, and Mach $= 0.83$ with $C_L = 0.25$. For each of the design points, both Mach number and lift coefficient are held fixed. In order to demonstrate the advantage of a multipoint design approach, the final solution at the middle design point will be compared with a single point design at the same conditions. As the geometry of the wing is modified, the design algorithm computes new wing-fuselage intersections. The wing component is made up of six airfoil defining sections. Eighteen Hicks-Henne design variables are applied to five of these sections for a total of 90 design variables. The sixth section at the symmetry plane is not modified. Spar thickness constraints were also enforced on each defining station at the $x/c = 0.2$ and $x/c = 0.8$ locations. Maximum thickness was forced to be preserved at $x/c = 0.4$ for all six defining sections. To ensure an adequate included angle at the trailing edge, each section was also constrained to preserve thickness at $x/c = 0.95$. Finally, to preserve leading edge bluntness, the upper surface of each section was forced to maintain its height above the camber line at $x/c = 0.02$. Combined, a total of 30 linear geometric constraints were imposed on the configuration.

Figures 5 – 7 show the initial and final airfoil geometries and C_p distributions after 5 NPSOL design iterations. It is evident that the new design has significantly reduced the shock strengths on both upper and lower wing surfaces at all design points. The transitions between design points are also quite smooth. For comparison purposes, a single point drag minimization study (Mach $= 0.81$ and $C_L = 0.25$) is carried out starting from the same initial configuration and using the same design variables and geometric constraints.

Figures 8 – 10 show comparisons of the solutions from the three-point design with those of the single point design. Interestingly, the upper surface

shapes for both final designs are very similar. However, in the case of the single point design, a strong lower surface shock appears at the Mach $= 0.83$, $C_L = 0.25$ design point. The three-point design is able to suppress the formation of this lower surface shock and achieves a 9 count drag benefit over the single point design at this condition. However, it has a 1 count penalty at the single point design condition. The three-point design features a weak single shock for one of the three design points and a very weak double shock at another design point. Table 1 summarizes the drag results for the two designs. The C_D values have been normalized by the drag of the initial configuration at the second design point. Figure 11 shows the surface of the configuration colored by the local coefficient of pressure, C_p, before and after redesign for the middle design point. One can clearly observe that the strength of the shock wave on the upper surface of the configuration has been considerably reduced.

Finally, Figure 12 shows the parallel scalability of the multiblock design method for the mesh in question using up to 32 processors of an SGI Origin2000 parallel computer. Despite the fact that the multigrid technique is used in both the flow and adjoint solvers, the demonstrated parallel speedups are outstanding.

Supersonic Constrained Aircraft Design

For supersonic design, provided that turbulent flow is assumed over the entire configuration, the inviscid Euler equations suffice for aerodynamic design since the pressure drag is not greatly affected by the inclusion of viscous effects. Moreover, flat plate skin friction estimates of viscous drag are often very good approximations. In this study, the generic supersonic transport configuration used in reference [36] is revisited.

The baseline supersonic transport configuration was sized to accommodate 300 passengers with a gross take-off weight of $750,000$ lbs. The supersonic cruise point is Mach 2.2 with a C_L of 0.105. Figure 13 shows that the planform is a cranked-delta configuration with a break in the leading edge sweep. The inboard leading edge sweep is 68.5 degrees while the outboard is 49.5 degrees. Since the Mach angle at $M = 2.2$ is 63 degrees it is clear that some leading edge bluntness may be used inboard without a significant wave drag penalty. Blunt leading edge airfoils were created with thickness ranging from 4% at the root to 2.5% at the leading edge break point. These symmetric airfoils were chosen to accommodate thick spars at roughly the 5% and 80% chord locations over the span up to

the leading edge break. Outboard of the leading edge break where the wing sweep is ahead of the Mach cone, a sharp leading edge was used to avoid unnecessary wave drag. The airfoils were chosen to be symmetric, biconvex shapes modified to have a region of constant thickness over the mid-chord. The four-engine configuration features axisymmetric nacelles tucked close to the wing lower surface. This layout favors reduced wave drag by minimizing the exposed boundary layer diverter area. However, in practice it may be problematic because of the channel flows occurring in the juncture region of the diverter, wing, and nacelle at the wing trailing edge.

The computational mesh on which the design is run has 180 blocks and $1,500,000$ mesh cells (including halos), while the underlying geometry entities define the wing with 16 sectional cuts and the body with 200 sectional cuts. In this case, where we hope to optimize the shape of the wing, care must be taken to ensure that the nacelles remain properly attached with diverter heights being maintained.

The objective of the design is to reduce the total drag of the configuration at a single design point (Mach $= 2.2$, $C_L = 0.105$) by modifying the wing shape. Just as in the transonic case, 18 design variables of the Hicks-Henne type are chosen for each wing defining section. Similarly, instead of applying them to all 16 sections, they are applied to 8 of the sections and then lofted linearly to the neighboring sections. Spar thickness constraints are imposed for all wing defining sections at $x/c = 0.05$ and $x/c = 0.8$. An additional maximum thickness constraint is specified along the span at $x/c = 0.5$. A final thickness constraint is enforced at $x/c = 0.95$ to ensure a reasonable trailing edge included angle. An iso-C_p representation of the initial and final designs is depicted in Figure 13 for both the upper and lower surfaces.

It is noted that the strong oblique shock evident near the leading edge of the upper surface on the initial configuration is largely eliminated in the final design after 5 NPSOL design iterations. Also, it is seen that the upper surface pressure distribution in the vicinity of the nacelles has formed an unexpected pattern. However, recalling that thickness constraints abound in this design, these upper surface pressure patterns are assumed to be the result of sculpting of the lower surface near the nacelles which affects the upper surface shape via the thickness constraints. For the lower surface, the leading edge has developed a suction region while the shocks and expansions around the nacelles have been somewhat reduced. Figure 14 shows the pressure coefficients and (scaled) airfoil sections for four sectional cuts along the wing. These cuts fur-

ther demonstrate the removal of the oblique shock on the upper surface and the addition of a suction region on the leading edge of the lower surface. The airfoil sections have been scaled by a factor of 2 so that shape changes may be seen more easily. Most notably, the section at 38.7% span has had the lower surface drastically modified such that a large region of the aft airfoil has a forward-facing portion near where the pressure spike from the nacelle shock impinges on the surface. The final overall pressure drag was reduced by 8%, from $C_D = 0.0088$ to $C_D = 0.0081$.

10   Conclusions

We have developed a three-dimensional control theory based design method for the Navier Stokes equations and applied it successfully to the design of wings in transonic flow. The method represents an extension of our previous work on design with the potential flow and Euler equations. The new method combines the versatility of numerical optimization methods with the efficiency of inverse design. The geometry is modified by a grid perturbation technique which is applicable to arbitrary configurations. Both the wing-body and multiblock version of the design algorithms have been implemented in parallel using the MPI (Message Passing Interface) Standard, and they both yield excellent parallel speedups. The combination of computational efficiency with geometric flexibility provides a powerful tool, with the final goal being to create practical aerodynamic shape design methods for complete aircraft configurations.

Acknowledgment

References

[1] R. M. Hicks, E. M. Murman, and G. N. Vanderplaats. An assessment of airfoil design by numerical optimization. *NASA TM X-3092*, Ames Research Center, Moffett Field, California, July 1974.

[2] R. M. Hicks and P. A. Henne. Wing design by numerical optimization. *Journal of Aircraft*, 15:407–412, 1978.

[3] J. L. Lions. *Optimal Control of Systems Governed by Partial Differential Equations.* Springer-Verlag, New York, 1971. Translated by S.K. Mitter.

[4] A. E. Bryson and Y. C. Ho. *Applied Optimal Control.* Hemisphere, Washington, DC, 1975.

[5] O. Pironneau. *Optimal Shape Design for Elliptic Systems.* Springer-Verlag, New York, 1984.

[6] A. Jameson. Optimum aerodynamic design using CFD and control theory. *AIAA paper 95-1729*, AIAA 12th Computational Fluid Dynamics Conference, San Diego, CA, June 1995.

[7] A. Jameson. Aerodynamic design via control theory. *Journal of Scientific Computing*, 3:233–260, 1988.

[8] A. Jameson and J.J. Alonso. Automatic aerodynamic optimization on distributed memory architectures. *AIAA paper 96-0409*, 34th Aerospace Sciences Meeting and Exhibit, Reno, Nevada, January 1996.

[9] A. Jameson. Re-engineering the design process through computation. *AIAA paper 97-0641*, 35th Aerospace Sciences Meeting and Exhibit, Reno, Nevada, January 1997.

[10] A. Jameson, N. Pierce, and L. Martinelli. Optimum aerodynamic design using the Navier-Stokes equations. *AIAA paper 97-0101*, 35th Aerospace Sciences Meeting and Exhibit, Reno, Nevada, January 1997.

[11] A. Jameson, L. Martinelli, and N. A. Pierce. Optimum aerodynamic design using the Navier-Stokes equations. *Theoret. Comput. Fluid Dynamics*, 10:213–237, 1998.

[12] A. Jameson. Automatic design of transonic airfoils to reduce the shock induced pressure drag. In *Proceedings of the 31st Israel Annual Conference on Aviation and Aeronautics, Tel Aviv*, pages 5–17, February 1990.

[13] A. Jameson. Optimum aerodynamic design via boundary control. In *AGARD-VKI Lecture Series, Optimum Design Methods in Aerodynamics*. von Karman Institute for Fluid Dynamics, 1994.

[14] J. Reuther, A. Jameson, J. J. Alonso, M. J. Rimlinger, and D. Saunders. Constrained multipoint aerodynamic shape optimization using an adjoint formulation and parallel computers. *AIAA paper 97-0103*, 35th Aerospace Sciences Meeting and Exhibit, Reno, Nevada, January 1997.

[15] J. Reuther, J. J. Alonso, J. C. Vassberg, A. Jameson, and L. Martinelli. An efficient multiblock method for aerodynamic analysis and design on distributed memory systems. *AIAA paper 97-1893*, June 1997.

[16] O. Baysal and M. E. Eleshaky. Aerodynamic design optimization using sensitivity analysis and computational fluid dynamics. *AIAA Journal*, 30(3):718–725, 1992.

[17] J.C. Huan and V. Modi. Optimum design for drag minimizing bodies in incompressible flow. *Inverse Problems in Engineering*, 1:1–25, 1994.

[18] M. Desai and K. Ito. Optimal controls of Navier-Stokes equations. *SIAM J. Control and Optimization*, 32(5):1428–1446, 1994.

[19] W. K. Anderson and V. Venkatakrishnan. Aerodynamic design optimization on unstructured grids with a continuous adjoint formulation. *AIAA paper 97-0643*, 35th Aerospace Sciences Meeting and Exhibit, Reno, Nevada, January 1997.

[20] J. Elliott and J. Peraire. 3-D aerodynamic optimization on unstructured meshes with viscous effects. *AIAA paper 97-1849*, June 1997.

[21] A. Jameson. Optimum aerodynamic design using CFD and control theory. AIAA Paper 95-1729-CP, 1995.

[22] A. Jameson. Optimum aerodynamic design using control theory. *Computational Fluid Dynamics Review*, pages 495–528, 1995.

[23] A. Jameson, W. Schmidt, and E. Turkel. Numerical solutions of the Euler equations by finite volume methods with Runge-Kutta time stepping schemes. *AIAA paper 81-1259*, January 1981.

[24] L. Martinelli and A. Jameson. Validation of a multigrid method for the Reynolds averaged equations. *AIAA paper 88-0414*, 1988.

[25] S. Tatsumi, L. Martinelli, and A. Jameson. A new high resolution scheme for compressible viscous flows with shocks. *AIAA paper* To Appear, AIAA 33nd Aerospace Sciences Meeting, Reno, Nevada, January 1995.

[26] A. Jameson. Analysis and design of numerical schemes for gas dynamics 1, artificial diffusion, upwind biasing, limiters and their effect on multigrid convergence. *Int. J. of Comp. Fluid Dyn.*, 4:171–218, 1995.

19

[27] P.L. Roe. Approximate Riemann solvers, parameter vectors, and difference schemes. *Journal of Computational Physics*, 43:357–372, 1981.

[28] A. Jameson. Analysis and design of numerical schemes for gas dynamics 2, artificial diffusion and discrete shock structure. *Int. J. of Comp. Fluid Dyn.*, 5:1–38, 1995.

[29] L. Martinelli. Calculations of viscous flows with a multigrid method. *Princeton University Thesis*, May 1987.

[30] A. Jameson. Multigrid algorithms for compressible flow calculations. In W. Hackbusch and U. Trottenberg, editors, *Lecture Notes in Mathematics, Vol. 1228*, pages 166–201. Proceedings of the 2nd European Conference on Multigrid Methods, Cologne, 1985, Springer-Verlag, 1986.

[31] J. J. Reuther, A. Jameson, J. J. Alonso, M. Rimlinger, and D. Saunders. Constrained multipoint aerodynamic shape optimization using an adjoint formulation and parallel computers: Part i. *Journal of Aircraft*, 1998. Accepted for publication.

[32] J. J. Reuther, A. Jameson, J. J. Alonso, M. Rimlinger, and D. Saunders. Constrained multipoint aerodynamic shape optimization using an adjoint formulation and parallel computers: Part ii. *Journal of Aircraft*, 1998. Accepted for publication.

[33] J.P. Steinbrenner, J.R. Chawner, and C.L. Fouts. The GRIDGEN 3D multiple block grid generation system. Technical report, Flight Dynamics Laboratory, Wright Research and Development Center, Wright-Patterson Air Force Base, Ohio, July 1990.

[34] J. Reuther and A. Jameson. Aerodynamic shape optimization of wing and wing-body configurations using control theory. *AIAA paper 95-0123*, AIAA 33rd Aerospace Sciences Meeting, Reno, Nevada, January 1995.

[35] J. Gallman, J. Reuther, N. Pfeiffer, W. Forrest, and D. Bernstorf. Business jet wing design using aerodynamic shape optimization. *AIAA paper 96-0554*, 34th Aerospace Sciences Meeting and Exhibit, Reno, Nevada, January 1996.

[36] J. Reuther, J.J. Alonso, M.J. Rimlinger, and A. Jameson. Aerodynamic shape optimization of supersonic aircraft configurations via an adjoint formulation on parallel computers. *AIAA paper 96-4045*, 6th AIAA/NASA/ISSMO Symposium on Multidisciplinary Analysis and Optimization, Bellevue, WA, September 1996.

Design	Conditions	Initial	Single Point Design	Three Point Design
Mach	C_L	Relative C_D	Relative C_D	Relative C_D
0.81	0.35	1.00257	0.85003	0.85413
0.82	0.30	1.00000	0.77350	0.77915
0.83	0.25	1.08731	0.81407	0.76836

Table 1: Drag Reduction for Single and Multipoint Designs.
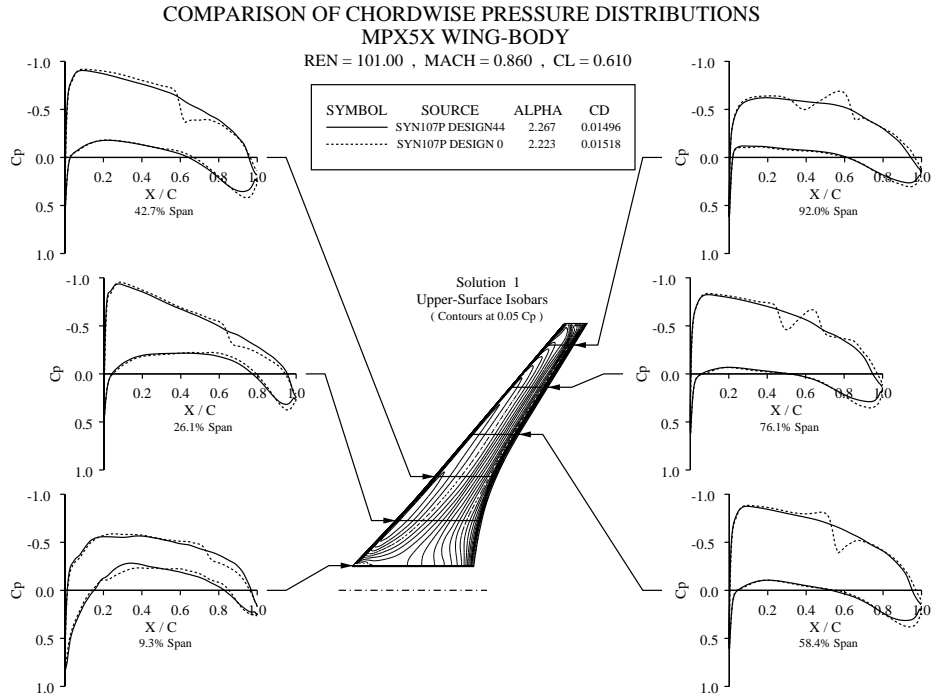
Figure 2: Pressure distribution of the MPX5X before and after optimization.

COMPARISON OF CHORDWISE PRESSURE DISTRIBUTIONS
MPX5X WING-BODY

REN = 101.00 , CL = 0.610

SYMBOL	SOURCE	MACH	ALPHA	CD
	SYN107P DESIGN 44	0.860	2.267	0.01496
	SYN107P DESIGN 44	0.855	2.355	0.01523
	SYN107P DESIGN 44	0.850	2.419	0.01535
	SYN107P DESIGN 44	0.840	2.518	0.01494
	SYN107P DESIGN 44	0.830	2.607	0.01463

Solution 1
Upper-Surface Isobars
(Contours at 0.05 Cp)
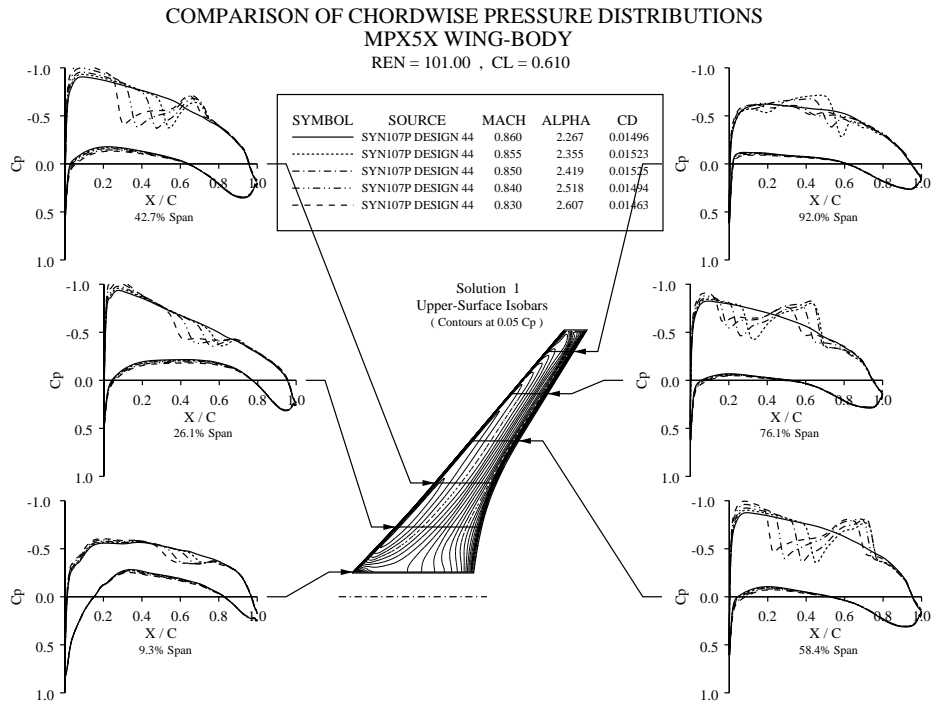
Figure 3: Off design performance of the MPX5X below the design point.

COMPARISON OF CHORDWISE PRESSURE DISTRIBUTIONS
MPX5X WING-BODY

REN = 101.00 , CL = 0.610

SYMBOL	SOURCE	MACH	ALPHA	CD
	SYN107P DESIGN 44	0.860	2.267	0.01496
	SYN107P DESIGN 44	0.865	2.201	0.01530
	SYN107P DESIGN 44	0.870	2.130	0.01596
	SYN107P DESIGN 44	0.880	2.008	0.01807

Solution 1
Upper-Surface Isobars
(Contours at 0.05 Cp)
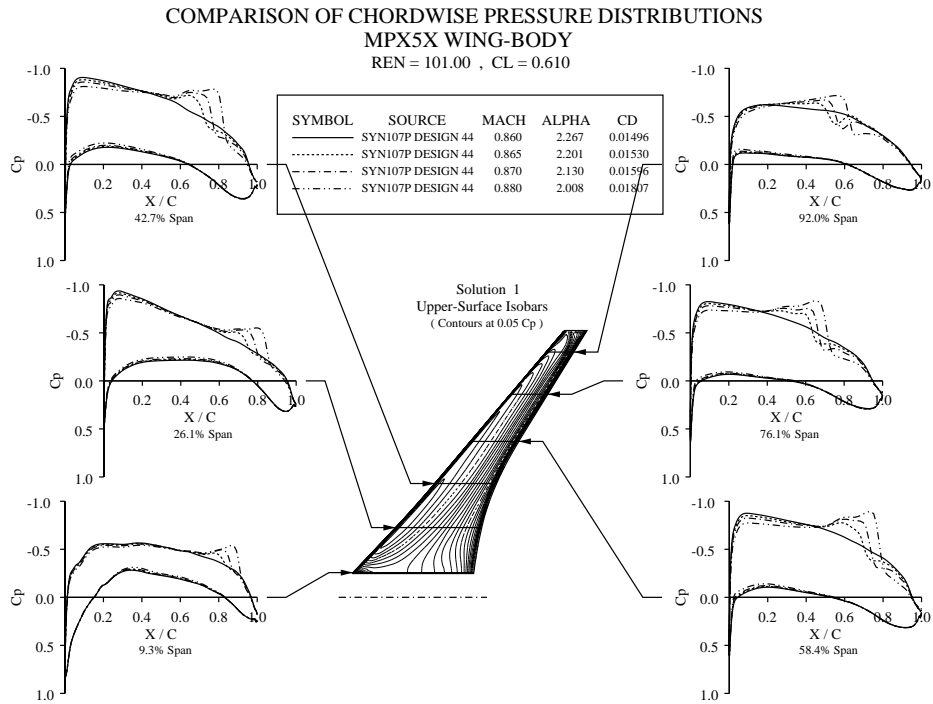
Figure 4: Off design performance of the MPX5X above the design point.
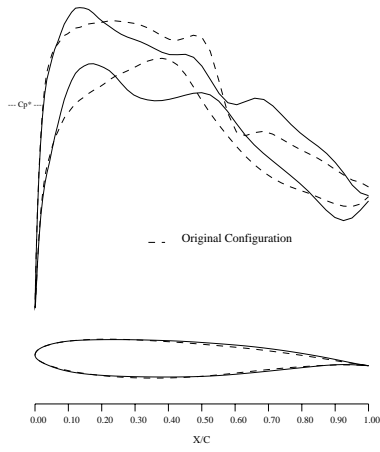
5a: span station $z = 0.190$
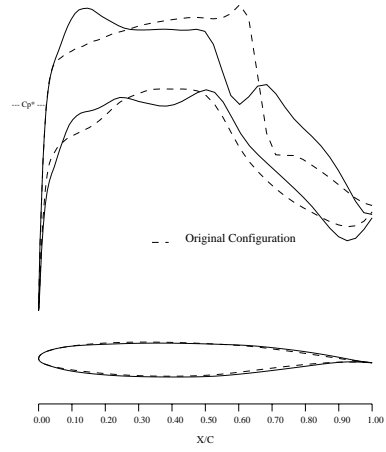
5b: span station $z = 0.475$
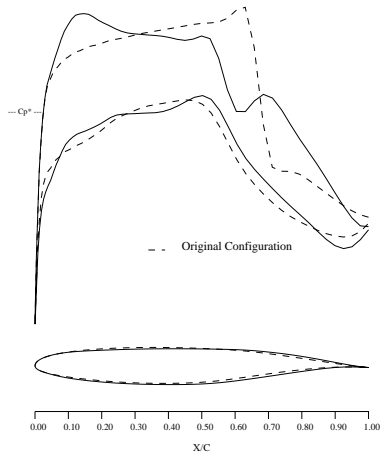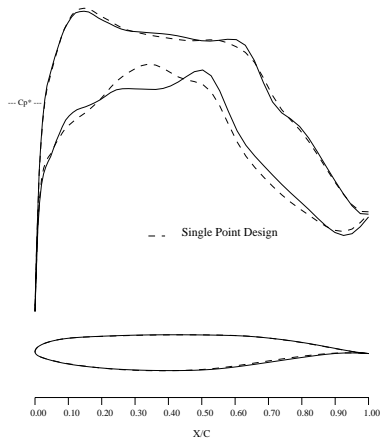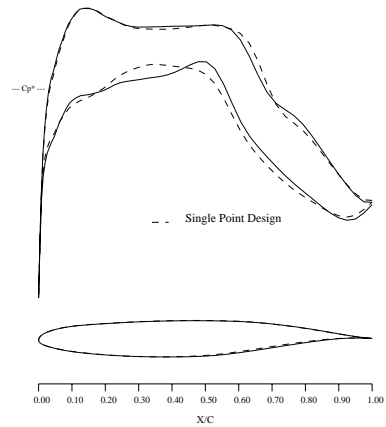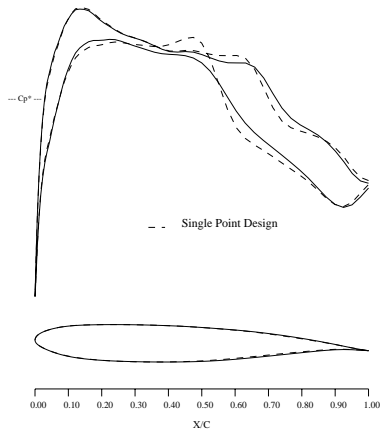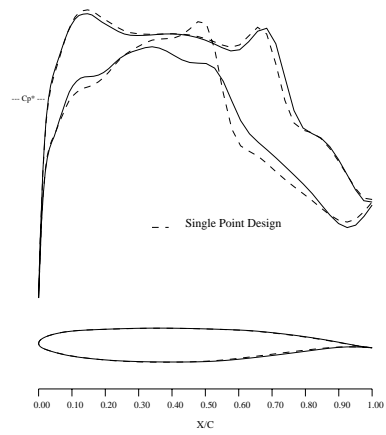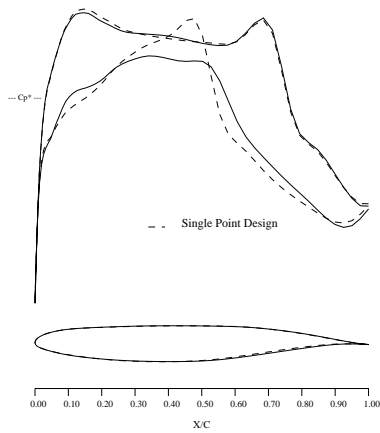

5c: span station $z = 0.665$
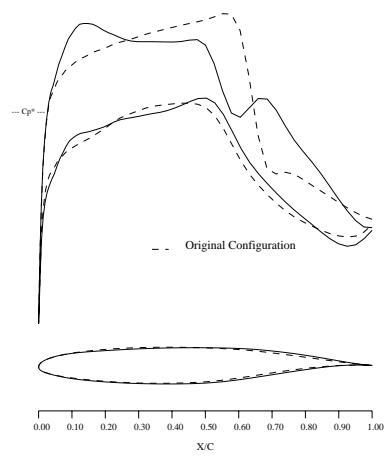
5d: span station $z = 0.856$

Figure 5: Business Jet Configuration. Multipoint Drag Minimization at Fixed Lift.
Design Point 1, $M = 0.81$, $C_L = 0.35$
90 Hicks-Henne variables. Spar Constraints Active.
$-\ -\ -$, Initial Pressures
————, Pressures After 5 Design Cycles.
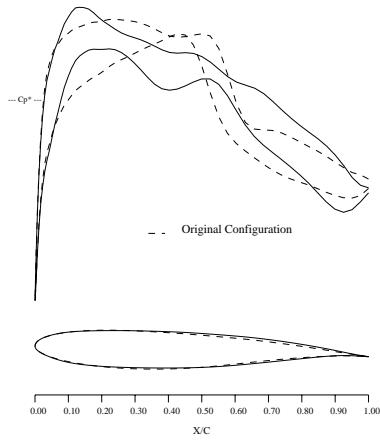
6a: span station $z = 0.190$
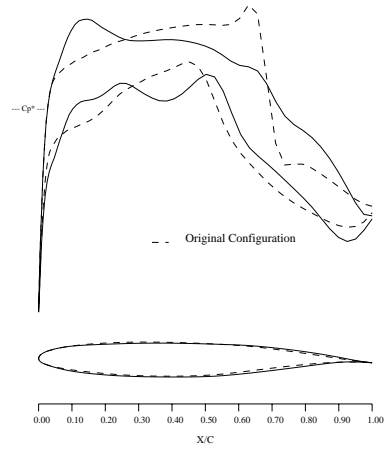
6b: span station $z = 0.475$
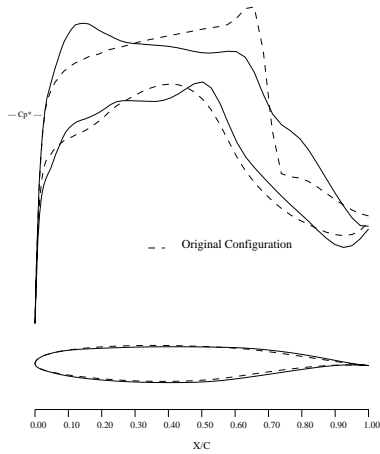
6c: span station $z = 0.665$
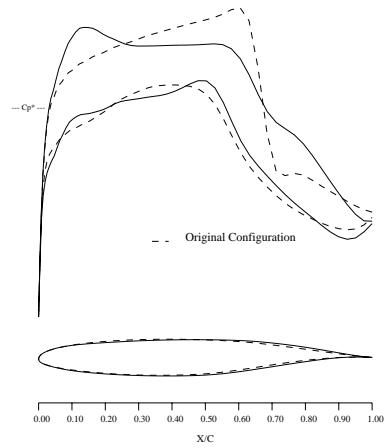
6d: span station $z = 0.856$

Figure 6: Business Jet Configuration. Multipoint Drag Minimization at Fixed Lift.
Design Point 2, $M = 0.82$, $C_L = 0.30$
90 Hicks-Henne variables. Spar Constraints Active.
$- \ - \ -$, Initial Pressures
————, Pressures After 5 Design Cycles.
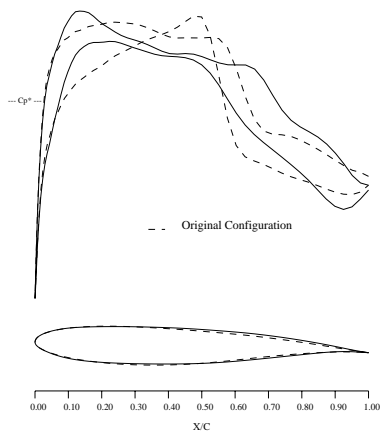
7a: span station $z = 0.190$
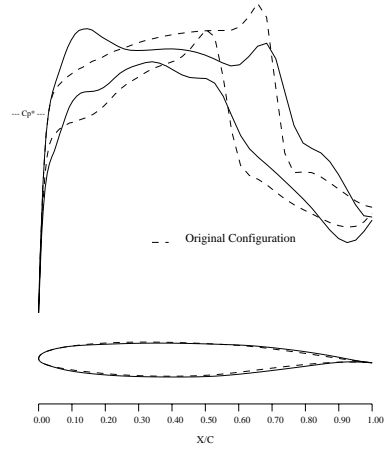
7b: span station $z = 0.475$
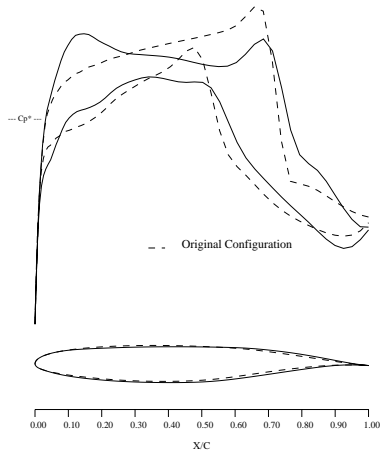
7c: span station $z = 0.665$
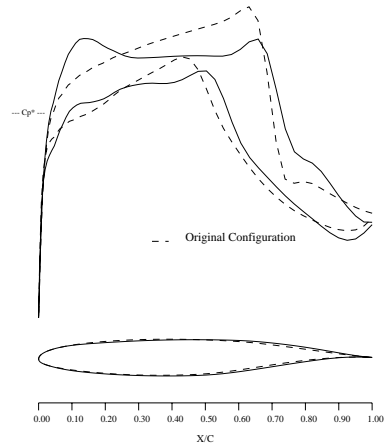
7d: span station $z = 0.856$

Figure 7: Business Jet Configuration. Multipoint Drag Minimization at Fixed Lift.
Design Point 3, $M = 0.83$, $C_L = 0.25$
90 Hicks-Henne variables. Spar Constraints Active.
$- - -$, Initial Pressures
———, Pressures After 5 Design Cycles.
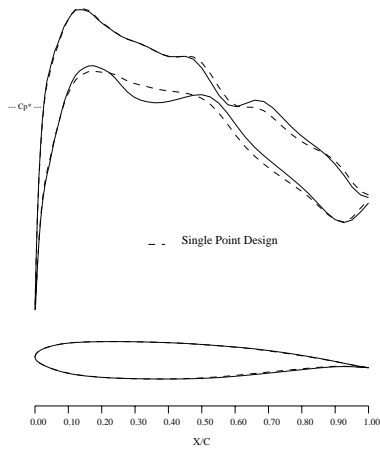
8a: span station $z = 0.190$
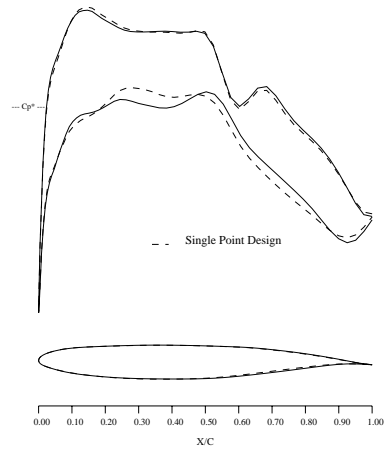
8b: span station $z = 0.475$
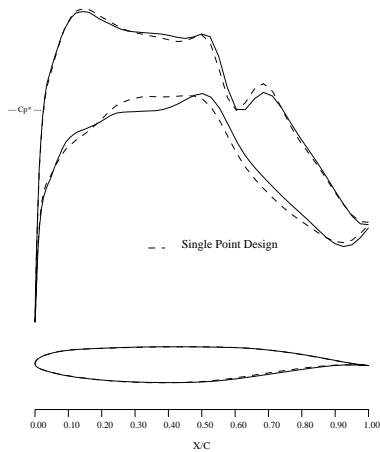
8c: span station $z = 0.665$
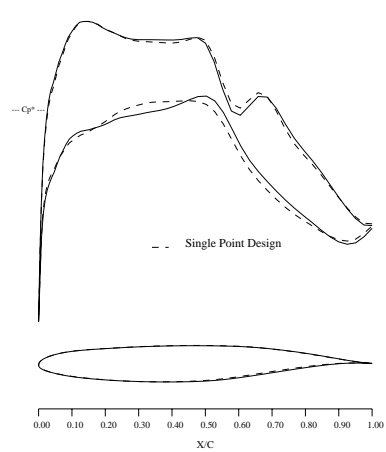
8d: span station $z = 0.856$

Figure 8: Business Jet Configuration. Single Point vs. Multipoint Drag Minimization at Fixed Lift. Design Point 1, $M = 0.81$, $C_L = 0.35$
90 Hicks-Henne variables. Spar Constraints Active.
$-$ $-$ $-$, Single Point Design Pressures.
————, Multipoint Design Pressures.
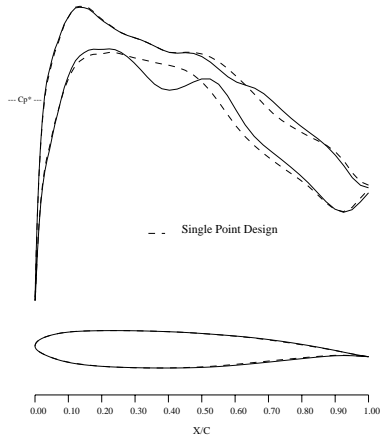
9a: span station $z = 0.190$
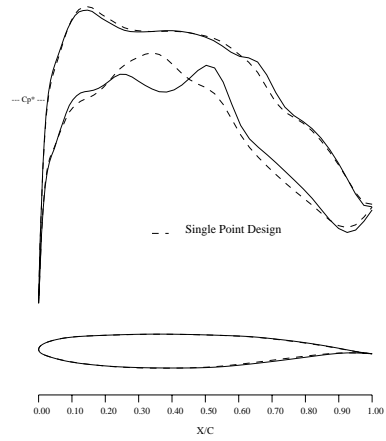
9b: span station $z = 0.475$

9c: span station $z = 0.665$

9d: span station $z = 0.856$

Figure 9: Business Jet Configuration. Single Point vs. Multipoint Drag Minimization at Fixed Lift.
Design Point 2, $M = 0.82$, $C_L = 0.30$
90 Hicks-Henne variables. Spar Constraints Active.
$- - -$, Single Point Design Pressure.
————, Multipoint Design Pressures.

10a: span station $z = 0.190$

10b: span station $z = 0.475$

10c: span station $z = 0.665$
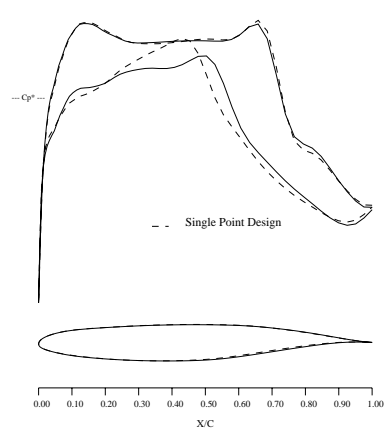
10d: span station $z = 0.856$

Figure 10: Business Jet Configuration. Single Point vs. Multipoint Drag Minimization at Fixed Lift.
Design Point 3, $M = 0.83$, $C_L = 0.25$
90 Hicks-Henne variables. Spar Constraints Active.
$- - -$, Single Point Design Pressures.
———, Multipoint Design Pressure.
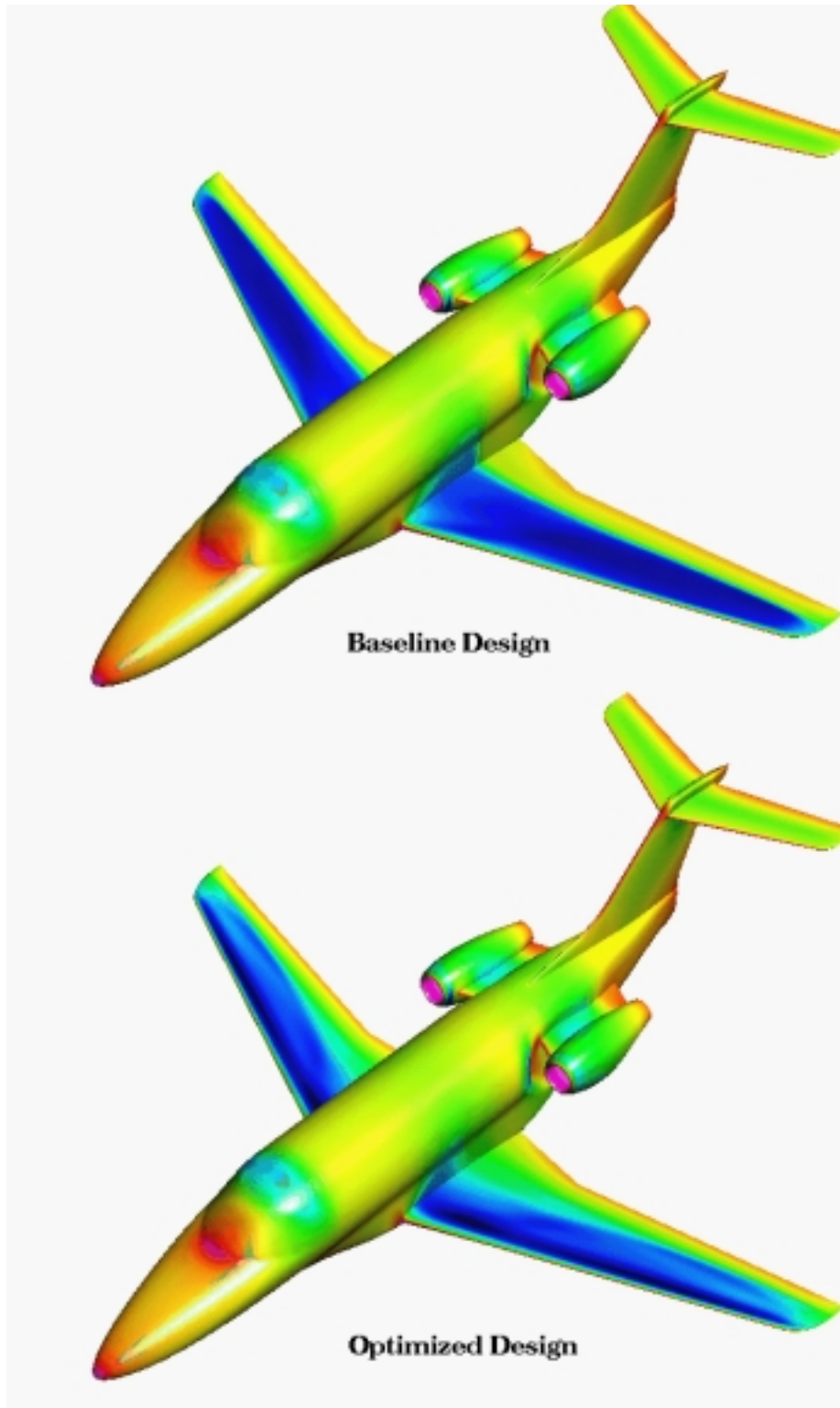
Figure 11: Geometry Surface Colored by local C_p Before and After Redesign.
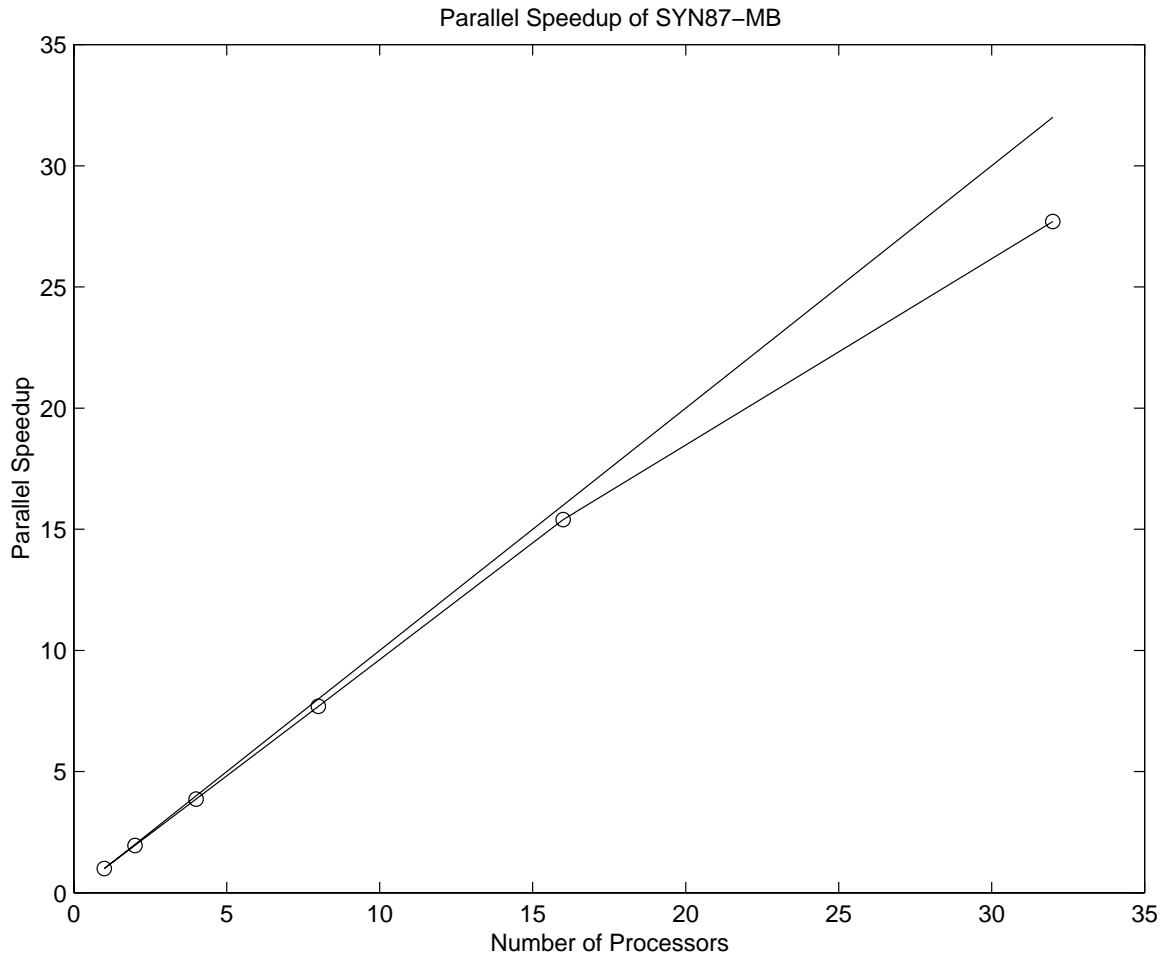
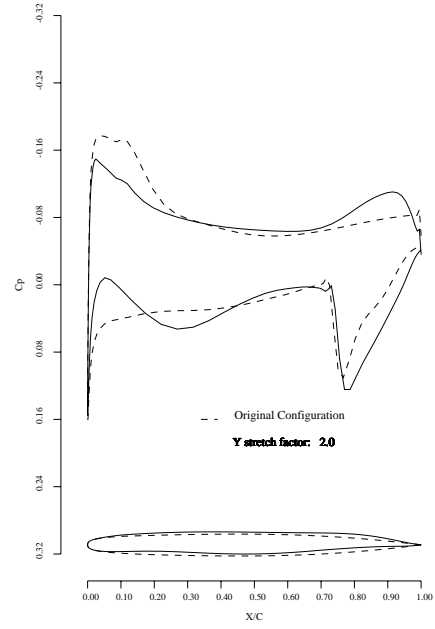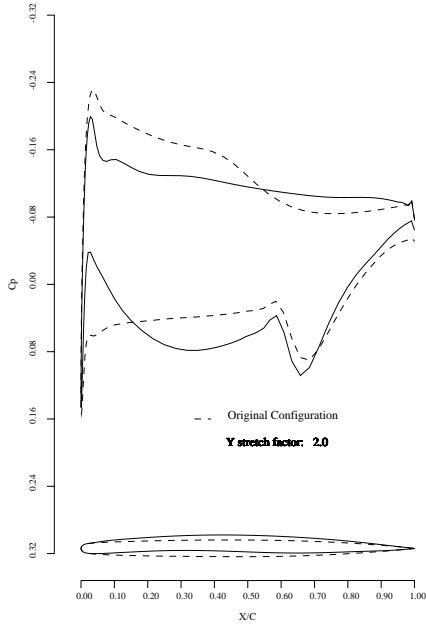Figure 12: Scalability Study for Multiblock Design Method.
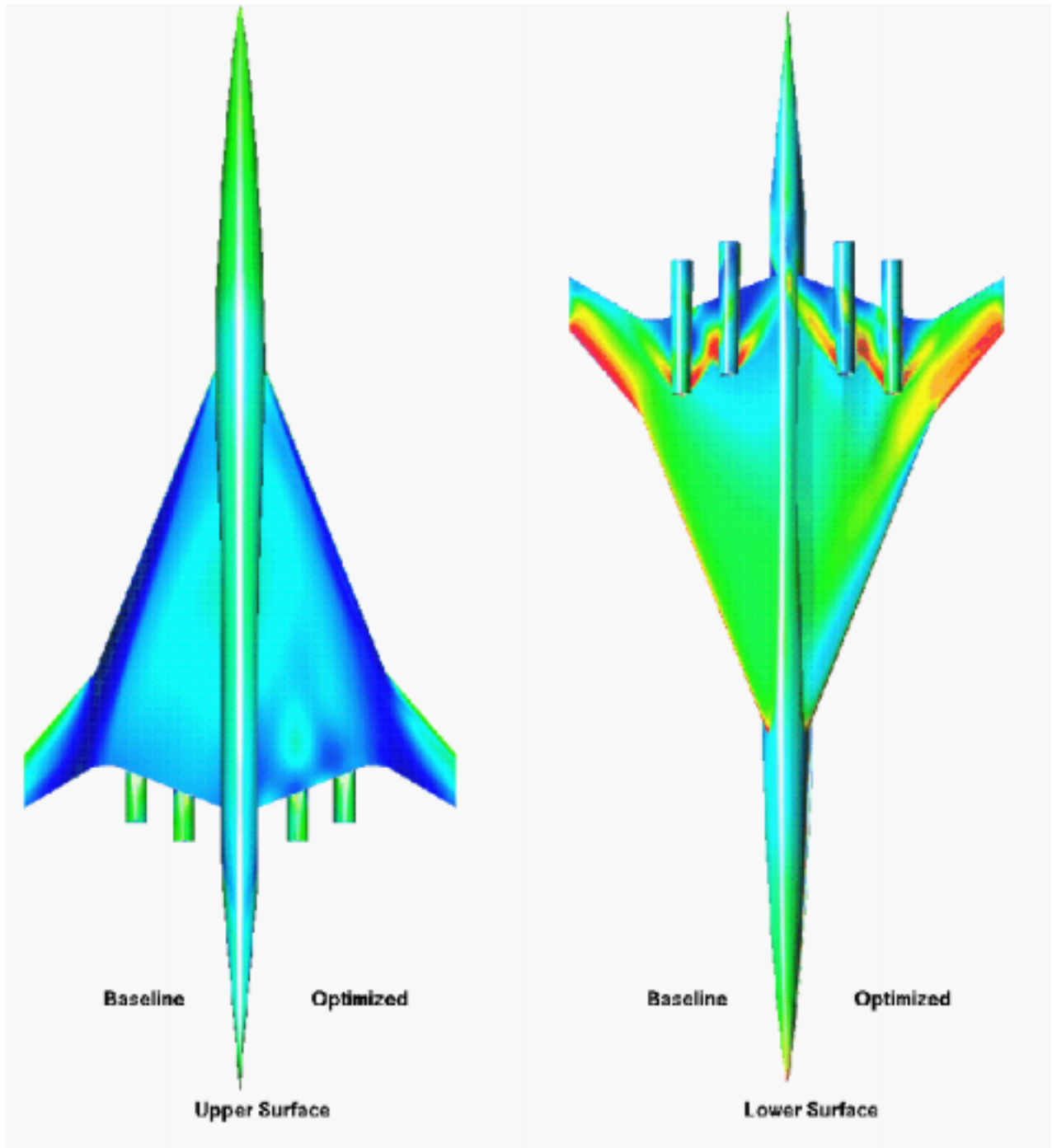
Figure 13: Supersonic Transport Configuration. Iso-C_p Contours on Upper and Lower Surfaces. Baseline and Optimized Designs. $M = 2.2$, $C_L = 0.105$.
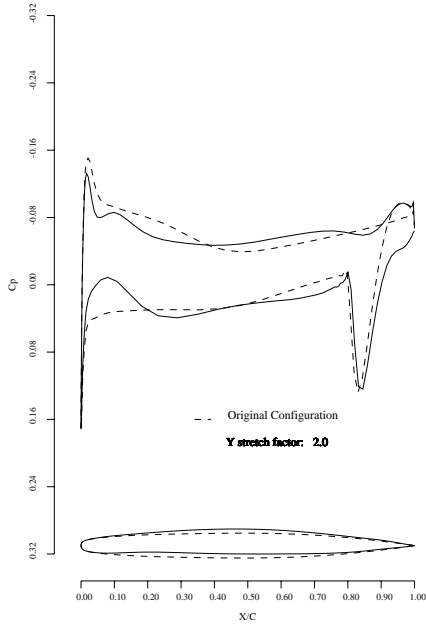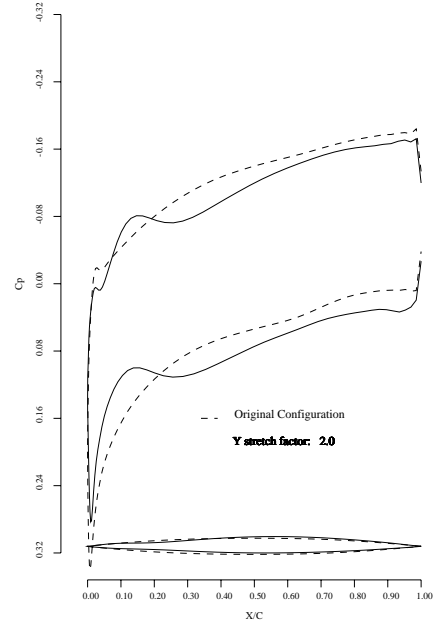
14a: span station $z = 0.194$

14b: span station $z = 0.387$

14c: span station $z = 0.581$

14d: span station $z = 0.775$

Figure 14: Supersonic Transport Configuration. Drag Minimization at Fixed Lift.
$M = 2.20, C_L = 0.105$
144 Hicks-Henne variables. Spar Constraints Active.
$- \ - \ -$, Initial Pressures
————, Pressures After 5 Design Cycles.